RÉPUBLIQUE ALGÉRIENNE DÉMOCRATIQUE ET POPULAIRE
MINISTÈRE DE L'ENSEIGNEMENT SUPÉRIEUR ET DE LA RECHERCHE
SCIENTIFIQUE
UNIVERSITÉ IBN KHALDOUN DE TIARET.

FACULTÉ DES SCIENCES APPLIQUÉES
DÉPARTEMENT GÉNIE ELECTRIQUE

Thèse de doctorat en Electrotechnique
Option: **Commandes Electriques**

Présentée par**:**
Khattab Khadidja

CONTRIBUTION A LA COMMANDE DES CONVERTISSEURS DC-DC DANS UNE PERSPECTIVE DE L'AMELIORATION DE LA QUALITE D'ENERGIE

SEBAA Morceli	Président	Pr à l'université de Tiaret
MESSLEM Youcef	Encadrant	Pr à l'université de Tiaret
SAFA Ahmed	Co- Encadrant	MCA à l'université de Tiaret
MIHOUB Youcef	Examinateur	MCA à l'université de Tiaret
TEJINI Hamza	Examinateur	Pr à l'université de Bechar
BOUDIAF Mohamed	Examinateur	Pr à l'université de Djelfa

25/01/2025

Doctoral thesis in Electrotechnics
Option: **Electrical Controls**

Presented by:
Khattab Khadidja

CONTRIBUTION TO THE CONTROL OF DC-DC CONVERTERS WITH A VIEW TO IMPROVE POWER QUALITY

SEBAA Morceli	President	Pr at Tiaret University
MESSLEM Youcef	Supervisor	Pr at Tiaret University
SAFA Ahmed	Co-Supervisor	MCA at Tiaret University
MIHOUB Youcef	Examiner	MCA at Tiaret University
TEJINI Hamza	Examiner	Pr at Bechar University
BOUDIAF Mohamed	Examiner	Pr at Djelfa University

25/01/2025

DEDICATION

I dedicate this work

To the memory of my father, whose unwavering support and

wisdom have guided me through every challenge.

To my mother, whose love and encouragement have been a

constant source of strength.

To my husband, whose patience, understanding, and love have

been my foundation.

To my brothers, for their companionship, humor,

and belief in me.

Each of you has shaped me in ways words cannot fully express,

and this achievement is as much yours as it is mine.

TABLE OF CONTENTS

TABLE OF CONTENTS

TABLE OF CONTENTS

TABLE OF CONTENTS

Nomenclatures

L_1 Inductor of the feeder boost converter

L_2 Inductor of the load boost converter

C_1 Capacitor of the feeder boost converter

C_2 Capacitor of the load boost converter

R_2 Resistor of the load boost converter

u_1 IGBT control of the feeder converter

u_2 IGBT control of the load converter

D_1 Duty cycle of the feeder converter

V_{in} Input voltage source

V_{in2} Input voltage of the load converter

V_{out1} Output voltage of the feeder converter

V_{out2} Output voltage of the load converter

I_{L1} Current through L_1

I_{L2}, i_{CPL} Current through L_2

u_{eq} Equivalent control

u_d Switching control

γ, λ parameters of super twisting control

NOMENCLATURES

s	Sliding surface
I_{ref1}	Desired inductor current of the feeder converter
$I_{ref\,2}$	Desired inductor current of the load converter
i_{out1}	Output current of the feeder boost converter
f_{d1}	Switching frequency of the feeder boost converter
f_{d2}	Switching frequency of the load converter

LIST OF FIGURES

LIST OF FIGURES

LIST OF FIGURES

LIST OF TABLES

LIST OF TABLES

Introduction

The growing adoption of DC microgrids in modern power systems stems from their suitability for renewable energy integration, high-efficiency energy conversion, and compatibility with emerging technologies such as electric vehicles and energy storage systems. These microgrids are fundamental in addressing the increasing global demand for reliable, sustainable, and decentralized power solutions. Within this context, the quality of power delivered by DC microgrids plays a crucial role in ensuring the stability, performance, and longevity of connected devices and systems. Among the various challenges faced by these systems, maintaining high power quality under the influence of nonlinear and dynamic loads, such as constant power loads (CPLs), remains a significant concern [1].

From a theoretical perspective, the control of DC-DC converters, as essential building blocks of DC microgrids, has emerged as a critical avenue for addressing power quality issues. These converters not only regulate voltage levels but also play a decisive role in minimizing disturbances caused by CPLs, which are known for their destabilizing effect on microgrid dynamics. On a practical level, ensuring optimal performance of these converters is vital for the seamless operation of renewable energy systems, efficient power distribution, and robust load management in modern power architectures [2].

Challenges Posed by Constant Power Loads (CPLs)

However, the presence of CPLs poses a key unresolved problem: their inherent negative incremental impedance destabilizes the system, leading to severe oscillations and degradation in power quality. Despite extensive research on control strategies for DC-DC converters, there remains a lack of effective solutions that comprehensively mitigate these issues while ensuring stability and high performance in real-world microgrid applications. This thesis addresses this gap by developing advanced control strategies aimed at improving power quality in DC microgrids, particularly in the presence of CPLs, thereby contributing to the broader goals of efficient and reliable energy systems [3].

System performance can be impacted by a CPL in any of the four cascaded configurations shown below [4]:
- A DC/DC converter upstream and a tightly regulated DC/DC voltage regulator.

1

- A strictly regulated inverter with an upstream DC/DC converter;
- A strictly regulated inverter with an input LC filter;
- A strictly regulated DC/DC voltage regulator with an input LC filter.

Existing Solutions for CPL-Induced Instability

In terms of mitigating the destabilizing effects of constant power loads (CPLs) in DC microgrids, previous research has focused on developing advanced control strategies and stabilization techniques to address their negative incremental impedance, which leads to instability and poor power quality. These solutions fall into three main categories: active techniques, passive techniques, and novel converter topologies. In the context of passive damping techniques, a method called inductor core biasing technique (ICBT) can reduce current ripple in DC-DC converters without increasing inductance value [5]. It has been proven that the suggested ICBT can substantially decrease the necessary inductance value to attain the same ripple current while enhancing saturation capability and efficiency for a given core size. However, it should be noted that this approach requires an additional circuit, which may increase the expenses and dimensions of the overall setup. In [6], an effective solution is proposed for replacing large capacitors in DC systems using a bidirectional buck-boost converter and an additional capacitor designed to eliminate ripples. The approach recommends three control techniques for regulating the voltage of the supplementary capacitor. This method can operate seamlessly under a broad range of operating conditions, but it should be noted that it employs a relatively intricate circuit. A recent study, presents a novel design approach that prioritizes voltage stability and minimizes electrical current surges in cascaded buck converters. The proposed method involves identifying the most suitable combination of output filter parameters for load converters and the main DC bus voltage. With just a few initial parameters and an optimization process, designers can determine the final values for bus voltage and output filter parameters for converter one. Additionally, this approach allows for the evaluation of each variable's impact and facilitates selecting the optimal balance between stability and short-circuit energy. However, energy dissipation remains a challenge for this study and other similar research endeavors, as it tends to reduce efficiency [7]. Passive damping methods have power dissipation issues that can be avoided by opting for active damping methods. In [8], the effect of phase shift between duty cycles of two stage cascaded converters is analyzed, and found that a proper adjustment in the phase shift can reduce the RMS current ripple of the capacitor without affecting the normal converter operation or requiring additional sensing circuits. Besides,

it leads to an overall efficiency improvement. However, the control flowchart used to regulate the phase shift between the duty cycles of the two power stage converter switches can be complex. The work in [9] addresses current ripple reduction in power systems by analyzing its main sources and proposing mitigation methods. It identifies two key sources: 100-Hz bus voltage ripple and quantized error-induced ripple from low pulse-width modulation resolution. This paper introduces a small-signal model with PIDR control and HRPWM, achieving an 81.5% current ripple reduction in a 2-kW converter prototype. For the new converters topologies, researchers are developing a new high-voltage gain DC-DC boost converter to enhance Maximum Power Point Tracking (MPPT) systems for photovoltaic (PV) panels. This converter, utilized alongside an MPPT boost converter, addresses issues like insufficient voltage supply and voltage stress across power switches. By minimizing input current source ripples and boosting voltage gain, the proposed converter aims to improve efficiency and prolong the lifespan of PV panels and semiconductor devices [10]. The work in [11] explores a magnetically coupled-inductor SIDO (CI-SIDO) boost converter, highlighting its ability to reduce input current ripples. Unlike interleaved boosts, the CI-SIDO features two output voltages and uneven inductances, with ripple cancellation relying on both gate pulse adjustments and inductor design.

Proposed Advanced Control Strategy for DC Microgrids

Addressing the problem of destabilizing effects of constant power loads (CPLs) in DC microgrids is essential for ensuring the stable operation of renewable energy systems, which are vital for achieving global sustainability goals. Additionally, the adoption of DC microgrids is growing in high-demand sectors, such as data centers and electric transportation, where uninterrupted and high-quality power is crucial. If left unresolved, the destabilizing effects of CPLs could limit the widespread adoption of DC microgrids and hinder technological progress in these sectors. Developing advanced control strategies to stabilize CPLs not only enhances the operational reliability of DC microgrids but also supports the broader goals of efficient, sustainable, and decentralized energy systems.

The main assumption of this thesis is that the advanced control strategy, belonging to the active damping technique, exploiting the fundamental component of the inductor current and integrating it with super-twist sliding mode control (STSMC), will effectively reduce current ripple and improve the overall power quality of DC microgrids with constant power loads (CPL). The main

objective is to develop and validate this control strategy for cascaded DC-DC converters to stabilize microgrids and improve power quality, with particular emphasis on constant power loads.

This thesis contributes to improving power quality in DC microgrids by developing an innovative control strategy to mitigate input current ripple in constant power loads (CPLs). The proposed approach is based on an active current ripple damping technique that leverages the fundamental component of the inductor current and integrates it with the super-twisting sliding mode control (STSMC). This method enhances the power quality of CPLs while significantly reducing input current ripples. The effectiveness of the proposed strategy relies on the crucial selection of the sliding surface, determined by the filtered inductance current of a secondary boost converter. The effectiveness of the proposed approach is illustrated by the simulation and experimental results presented below.

Thesis Structure and Chapter Overview

The thesis is structured around four chapters:

In the first chapter, various definitions of DC microgrids are given, their advantages and disadvantages, their components are cited, and their modes of operation. In addition, a classification of dc-dc converters is given, citing the advantages and disadvantages of each. General information on power quality and various control techniques conclude this chapter. The chapter concludes with a - Critical review of the various existing techniques for minimizing current ripple in dc-dc converters, assessing their performance, complexity and applicability to microgrids.

The second chapter proposes a basic structure for a DC microgrid, comprising two cascaded boost converters. The dynamic model of each stage is given. Next, a cascaded PI controller is used for the source-side converter, which is current and voltage controlled. The load-side converter is controlled by three variants;

- A cascade PI regulator
- Sliding mode control
- Super torsion control

This chapter will end with a simulation under input voltage variation.

The third chapter is focused on the design of a new technique based on STC control and first harmonic extraction to efficiently minimize current ripples in cascaded dc-dc converters. The

theoretical model is developed and then verified by three simulation tests for two voltage levels.

The new technique proposed in this thesis is validated in the fourth chapter. In this chapter, an experimental prototype is set up in the LGEP laboratory to validate the proposed technique in three tests. The obtained results are summarized in a bar chart. This chapter ends with a table comparing our contribution with previous work.

Finally, the thesis is concluded with a general conclusion, which concludes with some perspectives for the present work.

CHAPTER 1: Extensive Literature Review

I.1 Introduction

In the first part of this chapter, the main elements of this thesis are presented. Firstly, a general overview of dc-dc microgrids, dc-dc converters, and power quality is given. Also, some control techniques of classical and advanced dc dc converters are described. This chapter is concluded with a critical review of the different existing techniques for the minimization of current ripples in dc-dc converters by assessing their performance, complexity, and applicability to dc microgrids.

I.2 DC Microgrids

I.2.1 Microgrid Definitions

Microgrids are described as "electricity distribution systems containing loads and distributed energy sources, such as distributed generators, storage devices, or controllable loads, that can be operated in a controlled, coordinated way, either while they are isolated from the main grid or while they are connected to the main power network, in grid-connected mode, or while they are islanded." [12]

I.2.2 Other Definitions

I.2.2.1 U.S. Department of Energy MicroGrid Exchange Group:

A MicroGrid is a group of interconnected loads and distributed energy resources within clearly defined electrical boundaries that acts as a single controllable entity with respect to the grid. A MicroGrid can connect and disconnect from the grid to enable it to operate in both grid-connected or island mode [13].

I.2.2.2 CIGRÉ C6.22 Working Group, MicroGrid Evolution Roadmap:

Microgrids are electricity distribution systems containing loads and distributed energy resources, (such as distributed generators, storage devices, or controllable loads) that can be operated in a controlled, coordinated way either while connected to the main power network or while islanded [13].

I.2.3 Benefits and Disadvantages of DC Microgrids

Compared to an ac microgrid, a dc microgrid may have several advantages [14-19]

I.2.3.1 Benefits

➢ Reactive power and frequency regulation do not require control.

- There are no grid synchronization problems.
- No problem with inrush current because there isn't a transformer.
- An inverter's conversion losses are decreased.
- Fault-ride thanks to its inherent capabilities.
- Less AC/DC conversions inside the system, which lowers power losses. Distributed generator synchronization is not required.
- When there is a blackout in the commercial grid, loads can be supplied with energy through the distribution line, but in order to achieve high local availability, redundant architectures with multiple power sources or local storage are essential.
- Fluctuations of generated power and also of the loads can be compensated through energy storage modules.
- The system does not require long transmission lines, or high capacity lines.
- In the DC system, a lesser number of power converters are required, making possible an optimization of the size and an improvement of the overall efficiency.
- DC distribution does not require synchronization like AC distribution.
- It can be directly or indirectly drawn from renewable energy sources and the grid
- No phase balancing is required.
- The investment in conductors, wires etc. are comparatively low when compared to AC distribution.
- It provides a more efficient distribution than its AC counterpart.
- Storage devices such as batteries and flywheels are inherently DC, which adds to the compatibility of the total system.
- DC systems are best suited for loads, which are electronic such as laptops and computers. Applications such as data centers, telecommunication systems have a great advantage if they are run in DC.
- DC distribution has very few conversion stages, which improves its overall efficiency.
- DC has high reliability when compared with AC as it has only a few stages, which are prone to failure.
- More power for the same cable size when compared to AC distribution.
- Lower investment cost and power conversion losses due to elimination of unnecessary AC/DC converters.

➢ Lower cable losses due to absence of skin effect.

➢ Higher reliability and resilience to utility-side disturbances.

➢ Elimination of the need for frequency, phase, and reactive power controllers.

➢ Most renewable energy resources, such as photovoltaic (PV) panels and fuel cells produce DC power. Even wind turbines, which intrinsically produce AC power, can be more conveniently integrated into a DC grid due to the absence of more power conversions.

➢ There is no need for reactive power management and frequency synchronization.

➢ Most of energy storage devices are also DC in nature. The battery technologies that are already provided with an internal DC-DC converter would be easily integrated to a DC bus with reduced cost and increased efficiency.

I.2.3.2 Disadvantages

DC distribution is still lacking in many areas, despite its numerous benefits. Right now, the safety elements of the DC distribution are the major sources of concern. Currently, DC distribution safety devices are not commonly accessible. Few businesses actually customize their products to meet the demands of their clients. 380V is the voltage level that is most commonly used in DC distribution since it is thought to be both high enough to lower conductor costs and low enough to ensure safe transmission. Currently, data centers and telecom buildings use it for power distribution. Because of this, more study is being done on safety devices for this voltage level as it becomes standardized.

The following problems affects the safety of the DC distribution:

➢ No zero cross over of voltage and current.

➢ Arc during switching.

➢ It is necessary to construct private dc distribution lines.

➢ Because dc systems lack a zero crossing point for current, protecting them is more difficult than protecting ac systems.

➢ Reactive power may manage the voltage of the ac system without impacting active power, whereas active power flow alone affects voltage stability.

I.3 Components of a Microgrid

The Microgrid is a physical network connected system including distributed generation units, storage, loads, and connections to other grids (AC or DC). It is operated by sophisticated control

techniques to regulate energy flow distribution and give data on energy use [20]. As seen in figure I.1, microgrids are generally composed by:
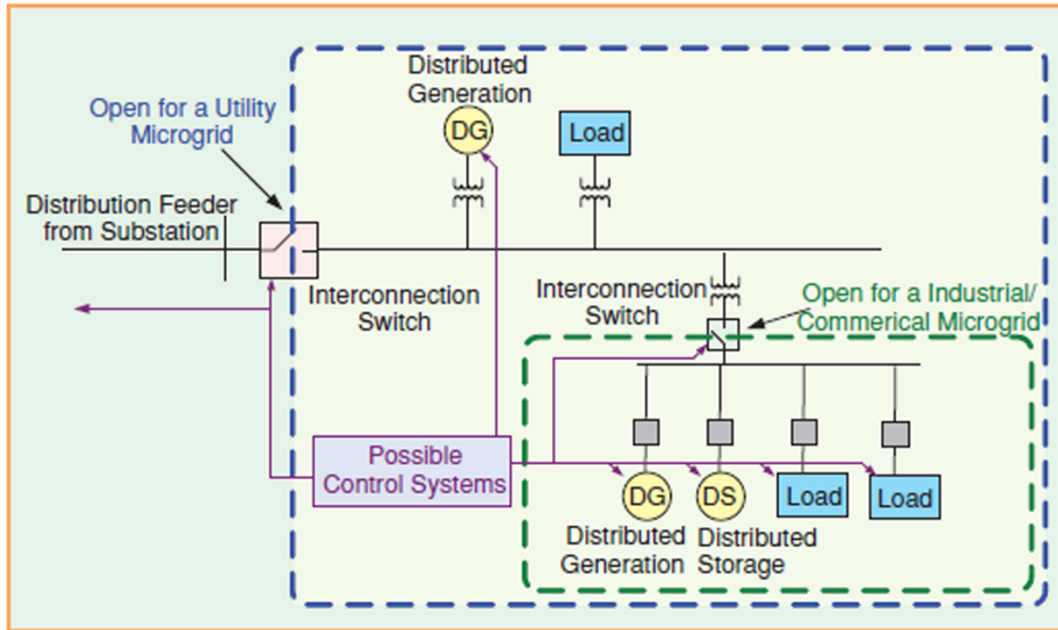
Figure I. 1. Components of microgrid

I.3.1   Distributed Generators

MicroGrids utilize diverse generation resources, including renewables like solar, wind, water, and biomass, alongside conventional distributed generators (DGs). Micro turbines are often used in combined heat and power (CHP) systems. DGs can operate as voltage source inverters (VSIs) for energy storage or current source inverters (CSIs) for sources requiring maximum power tracking, such as solar and wind. Environmentally friendly and cost-effective technologies are deployed at the MG level to meet local demands. Renewable energy resources (RERs) minimize environmental impact, transmission costs, and energy losses [21].

I.3.2   Distributed Storage

When distributed generation units produce more energy than required, storage systems are used to store the extra energy. This stored energy can then be used in the event of excess demand. Batteries, supercapacitors, pumped hydro and flywheels are examples of energy storage devices [22]. In order to improve Microgrid performance overall, distributed storage does two ways:

10

1. It stabilizes and allows distributed generation units to operate at a steady and consistent output, even in the face of load variations.

2. Enabling dispatchable unit DG to function as a unit with ease. Power systems can benefit from energy storage by allowing backup generators to respond to power outages, reducing transient power disruptions, storing energy for future use, and reducing peak spikes in electricity demand.

I.3.3 Loads

Microgrid customers include residential and commercial loads, classified as critical (e.g., hospitals) or non-critical, with priority given to critical loads for reliability. Loads are also categorized by linearity; non-linear loads (e.g., rectifiers) cause voltage distortions and harmonics. Prioritizing key loads is essential for Microgrid stability [17].

I.3.4 Control System

A microgrid's local voltage and frequency can be adjusted by the control system to ensure optimal operation in both linked and stand-alone modes. Systems with high-distributed energy resource penetration are susceptible to voltage and/or reactive power excursions and oscillations in the absence of efficient local voltage management. Minimizing reactive current flow between sources is crucial for voltage regulation [22].

I.3.5 Power Converters

Most DER microgrids need power converters in order to convert produced electricity into AC power that is suitable for the appliances. Power converters are used for power conversion, power conditioning, and output interface protection. For the microgrid to function as a single controlled unit, the majority of micro sources need a power electronic device [17].

I.4 Operation Mode of DC Microgrid

I.4.1 Islanded Mode of Operation

When the microgrid is in its islanded condition, it needs much more intricate control because it is not supported by the grid. At this stage, the microgrid's low system inertia makes it very vulnerable to changes in load and fluctuations in generation. The microgrid needs a stable power source in order to remain in an islanded condition. Electrostatic or electrochemical energy storage devices are usually used for this. In an island situation, stable voltage and frequency can be preserved through efficient management of storage devices such super capacitors and batteries. Because the

power distribution between the inverters of different generators is a critical issue for autonomous operation, a variety of control strategies, such as the master-slave control method, control area network communication, and voltage and frequency droop strategy based on local measurements, have been investigated in islanded MGs up to this point. Microgrids function in this mode as a result of grid maintenance or faults, or by taking economic factors into account. When in autonomous mode, which provides voltage and frequency set points, centralized or decentralized control can be employed. Short-distance distribution networks employ hierarchical source and load management under centralized control. Decentralized control is utilized when generation of energy is less than demand. In a decentralized mode, either master slave, droop control, or a combination of the two control systems can be used [23].

I.4.2   Grid Connected Mode of Operation

A static transfer switch connects the microgrid to the utility grid in this mode of operation. Point of common coupling (PCC) is the name given to the connection point. According to load and source conditions, the microgrid controller continually monitors the microgrid's generation and demand, exporting excess power or importing deficient power through the inverter. After connecting to the grid, the microgrid switches to P-Q control to manage active and reactive power, giving up control over the system's frequency and voltage [23].

I.5   DC-DC Converter: Principle and Topology

I.5.1   Classification of DC-DC Converters

As seen in figure I. 2, DC-DC converters are commonly classified into two groups: isolated and non-isolated [24]. Isolation could be required primarily for safety and grounding reasons. Isolation helps in the first case by keeping high-voltage (HV) from showing up on low-voltage (LV) terminals. This is an important factor to take into account, especially in applications where the transformation ratio is high. Different grounding approaches on both DC grids can be coupled in terms of grounding thanks to the isolated structures [25].
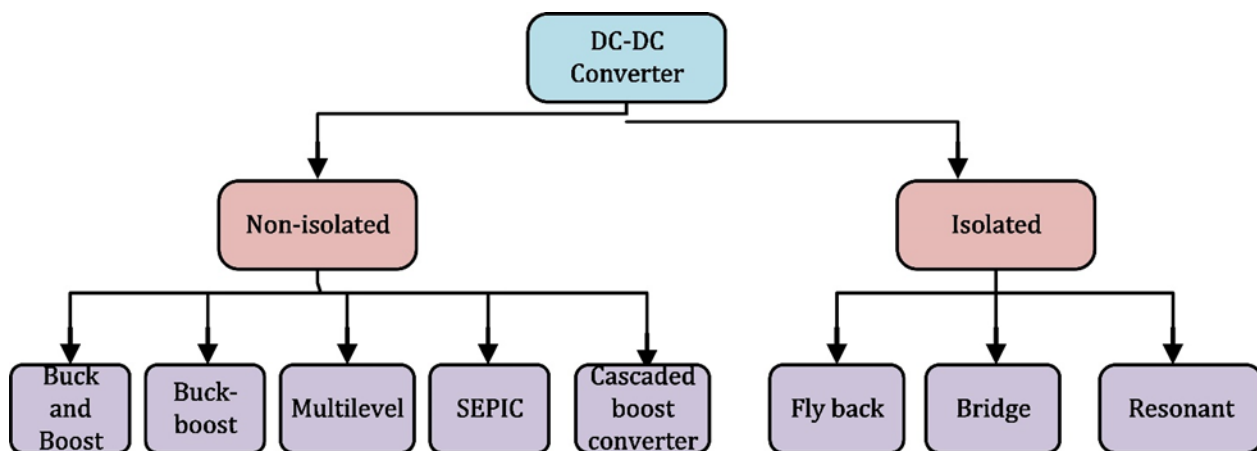
Figure I. 2. Classification of DC-DC converters

I.5.1.1 Buck and Boost Converter

The original buck and boost converter presented in figure I. 3, served as the foundation for the introduction of the basic bidirectional converter. An advancement in the unidirectional buck and boost converter allows for the realization of this bidirectional topology. In the other words, the bidirectional buck and boost-derived converter will be produced if the bidirectional power switches take the place of the unidirectional switches in the conventional buck and boost converter. When running in the other direction, the converter functions as a buck converter and boost converter from the LV to the HV [26].
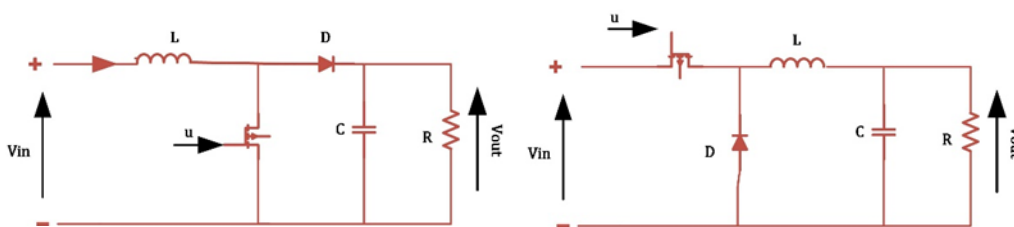
Figure I. 3. Buck and boost converters

I.5.1.2 Buck-Boost Converter

As seen in Figure I. 4, the buck-boost converter topology combines two distinct converter topologies. Two types of converters are available: the buck converter reduces the output voltage level while the boost converter increases it. Numerous applications, including driving applications, standalone, and grid-connected photovoltaic (PV) energy generation systems, use this hybrid converter topology. Still being researched, though, is the buck-boost converter topology and how it can improve the efficiency of photovoltaic (PV) energy generation systems. Due to efforts by

13

researchers worldwide to improve the voltage gain of non-isolated DC-DC converters, a variety of buck-boost topology-based DC-DC converters, including as SEPIC, Cuk, Lou, and Z-source, have been created [27].
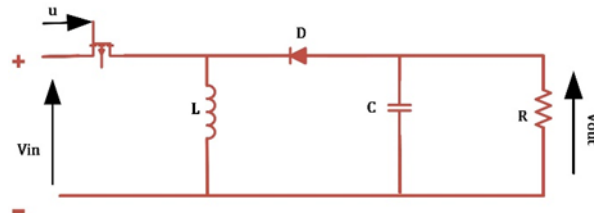
Figure I. 4. Buck-boost converter

I.5.1.3 *Single-Ended Primary Inductance Converter (SEPIC)*

Figure I. 5 depicts the single-ended primary inductance converter, also known as a SEPIC converter. In order to get a greater output voltage during switching, the ON duration must essentially be longer than the OFF time (due to the inductor's longer charging period). The converter stops producing the needed output if it doesn't. The capacitor is unable to charge to its full capacity. When designing the converter, a number of constraints must be taken into consideration. The output voltage ripple is intended to decrease when the traditional SEPIC converter is used in conjunction with a high-frequency transformer. Key properties of this configuration include constant output current, low switching stress, and low output ripple. Certain harmonics that were generated during the AC–DC conversion caused ripples in the AC currents, which ultimately decreased the power factor [28].
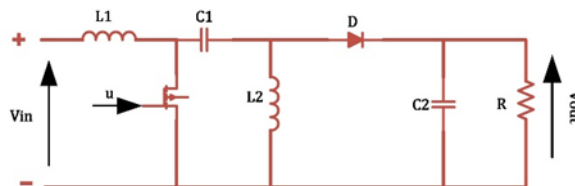
Figure I. 5. Single-Ended Primary Inductance Converter

I.5.1.4 *Cascaded Boost Converter*

The double cascade boost converter shown in Figure I. 6 results from the association of two identic elementary boosts connected in tandem. It consists of an input voltage source *Vin*, two independently controlled switches, two freewheeling diodes *D1* and *D2*, two capacitors *C1* and *C2* and two inductors *L1* and *L2*.
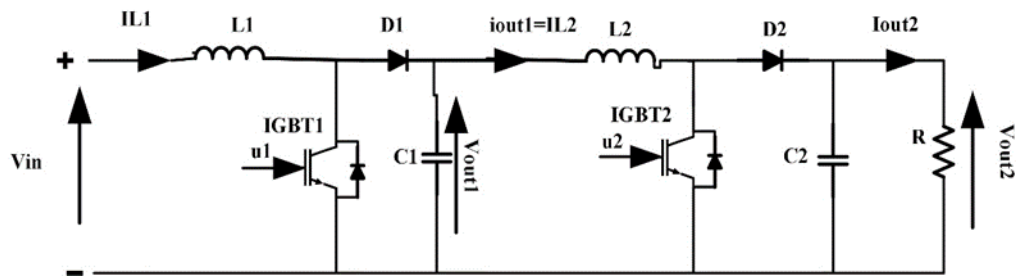
Figure I. 6. Cascaded dc-dc converter

I.5.1.5   Multilevel DC-DC Converter

A multilevel bidirectional DC-DC converter is depicted in Figure I. 7. To achieve a high voltage gain in this design, a switching module is employed as a repeating pattern in each level. Originally, the converter was employed in dual voltage automobile systems. This converter weighs and measures significantly less than ones that use magnetic elements since it does not include an inductor [26].
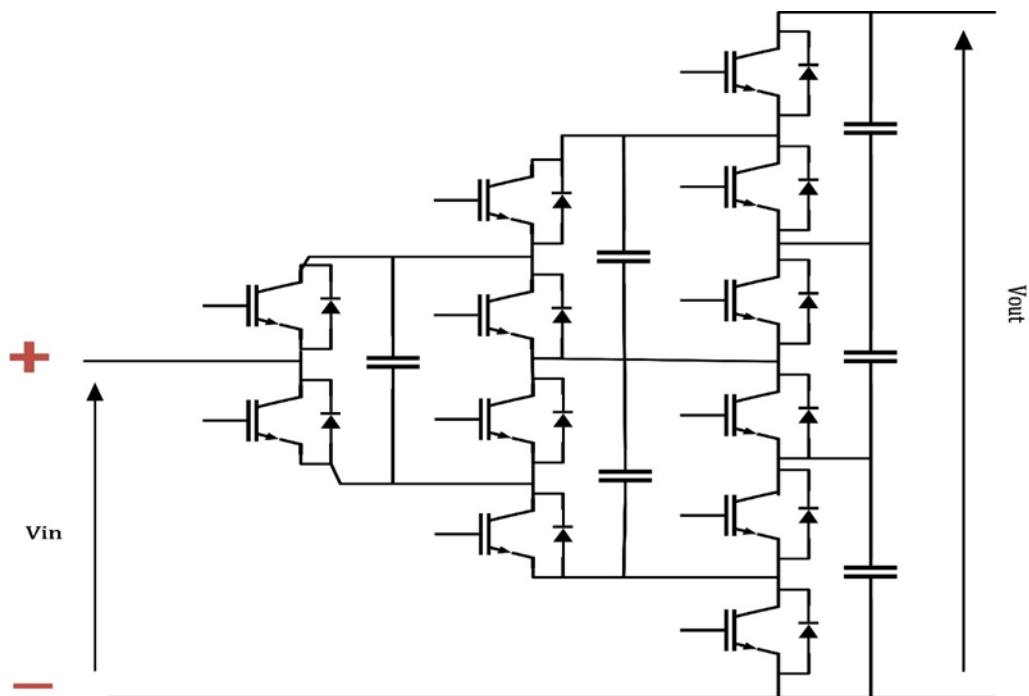
Figure I. 7. Multilevel dc-dc converter

I.5.1.6   Flyback Converter

The flyback converters, pictured in Figure I. 8, are mostly used in ultra-low power solar PV systems. Using flyback converters is the primary method whenever a larger converter gain is

15

required in addition to using transformers. In order to store energy, the transformer must have a big air gap for high power applications. The lower magnetizing inductance is caused by the huge airgap; flyback converters result in higher leakage flux and extremely low energy transfer efficiency. Despite being utilized in high-power applications, cuk converters have a few disadvantages, namely polarity [28].
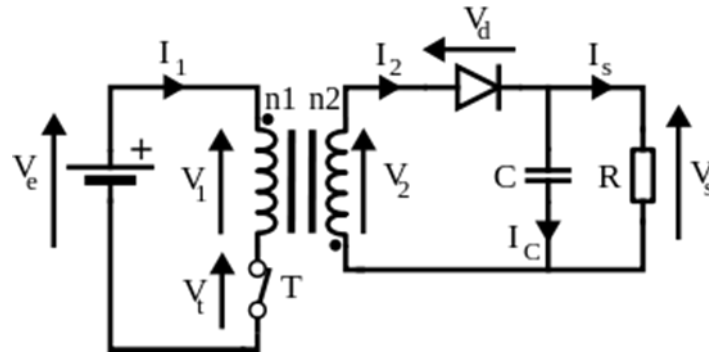
Figure I. 8. Flyback converter

I.5.1.7 *The Dual Active Bridge – Isolated Bidirectional DC–DC Converter*

Due to its key features—bidirectional power flow, high conversion efficiency, galvanic isolation, high power density, and inherent soft switching property—the Dual Active Bridge – Isolated Bidirectional DC–DC Converter (DAB-IBDC) topology, shown in Figure I. 9, is popular by researchers. The DAB-IBDC is a crucial circuit for standalone hybrid system applications thanks to these qualities. Using a high-frequency power transformer with leakage inductance that serves as an energy storage component, the two complete bridges are isolated. A low voltage energy storage device or load is connected to the secondary bridge, while the primary bridge is connected to a high voltage DC source. To allow for bidirectional power transfer, it is convenient to phase shift the square wave between the two bridges with regard to one another. Maintaining control over the voltage differential across the energy storage device allowed for the power conversion to occur [28].
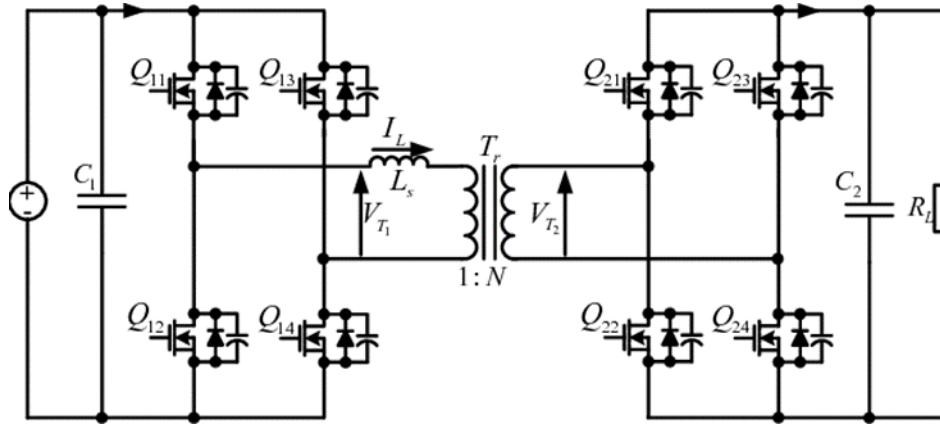
Figure I. 9. Dual Active Bridge – Isolated Bidirectional DC–DC Converter

I.5.1.8   Full Bridge Converter

In most renewable energy systems, a full-bridge converter is used to connect the renewable source, storage device, and load. Two buck-boost converters are integrated into the full-bridge topology through a full-bridge three-port converter. With this topology presented in figure I. 10, it is simple to create a single power conversion step and zero voltage switching for all available switches. For the purposes of the renewable energy system, an extremely effective asymmetrical pulse-width-modulated full-bridge converter was put into practice. This converter minimizes the circulating current loss by turning on switches that flip at zero voltage using an asymmetric control strategy and full-bride topology [28].
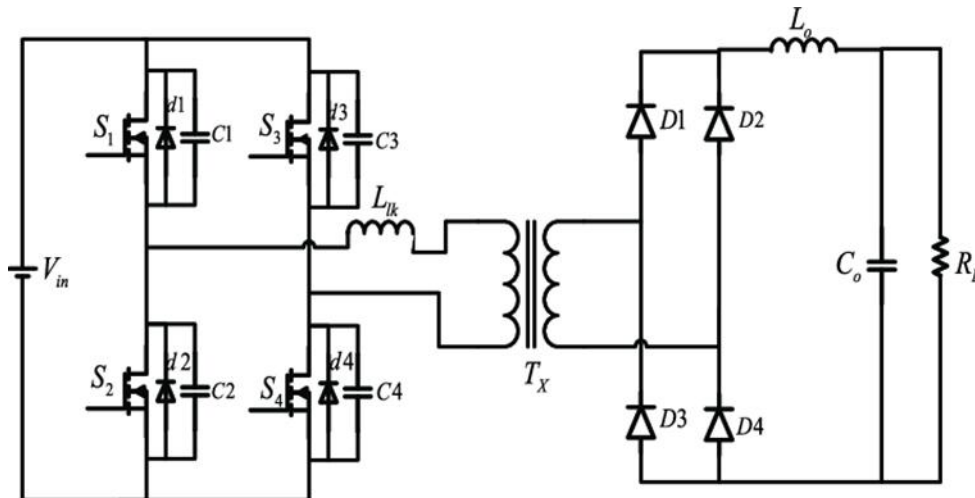
Figure I. 10. Full bridge converter

I.5.1.9 Half Bridge Converter

As seen in figure I. 11, a three-port half-bridge converter was created for use in renewable energy systems. The half-bridge converter's main circuit operates as a synchronous rectification-buck converter, enabling the high-frequency transformer to receive DC bias current. A synchronous regulation and a post-regulation with different implementations are anticipated. With the advantages of single-stage power conversion, minimal converter architecture, and straightforward control, it accomplishes independent regulation on three ports. A three-switch active-clamped half-bridge DC converter was put into practice. It achieves continuous input current with low ripple and wide range ZVS [28].
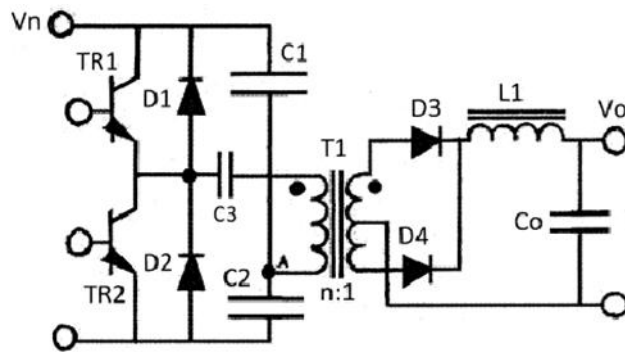
Figure I. 11. Half bridge converter

I.5.1.10 Resonant DC-DC Converter

On the primary side, the wide output voltage range resonant converter uses four different implementations. The LC notch and the LLC tank are combined to create the "five-element resonant tank based resonant converter," which increases the voltage gain by offering additional resonant frequencies. In order to enable two modes of operation, the "dual half-bridge based resonant converter" is built utilizing two half bridges and two resonant tanks. Phase shift is implemented between the input square voltages in the third approach, referred to as "multi-phase bridge based resonant converter," which is based on topology. The fourth technique, called "multiswitch bridge based resonant converter," is built by incorporating auxiliary switches onto the primary side, which allows the topology to function in various bridge configurations [29].

I.5.2 Advantages and Disadvantages of DC-DC Converters in Terms of Performance

The advantages and disadvantages of dc-dc converters in terms of performance are summarized in the table I. 1 [30-37].

18

Table I. 1. Advantages and disadvantages of dc-dc converters in terms of performance

Type of dc-dc converter	Advantages	Disadvantages
Boost	Simple switching Continuous input current Easy filtering Moderate efficiency Single polarity output Simple circuitry	Large output capacitor Limited high voltage gain
Buck	High Efficiency Simplicity Controllable Output Voltage	Output Voltage Ripple
Buck-boost	Versatility Duty Cycle Control	More complex compared to simpler buck or boost converters Potential for Lower Efficiency
Multilevel	Reduced Voltage Stress on Switches Lower Harmonic Distortion Scalability	Increased Component Count Complexity
SEPIC	output voltage polarity, voltage and current ripple voltage power gain The increasing and settling times are short	higher number of components
Cascaded boost converter	High voltage gain Reduced Stress on Components Reversible	Control Challenges CPL

Fly back	simple circuit topology few electronic components, low cost, easy control, high safety of input or output galvanic isolation, and good output voltage or current characteristics	Low efficiency
Bridge	Used high power applications Reasonable device voltage ratings	High conduction losses high number of components Current mode control is requiered to avoid the transformer saturation Low efficiency
resonant	smooth quasi-sinusoidal waveforms reduced switching losses increased efficiency reduced size and weight	Increased complexity Higher costs Generation of parasites

I.6 Power Quality

I.6.1 Definitions

The availability of a suitable definition that is sufficiently broad to cover both AC and DC power quality is the first issue when it comes to power quality. The definition given by IEC 61000 is appropriate in that regard since it states "Power quality encompasses the characteristics of the electricity at a given point on an electrical system, evaluated against a set of reference technical parameters" without distinguishing between AC and DC power [38]. Different definitions of power quality are given in other references, but none of them distinguishes between AC and DC power quality:

- ➢ The result of combining current and voltage quality is power quality. Power quality, thus, is concerned with voltage and/or current variations from the ideal waveform [39].
- ➢ Any power issue that causes variations in voltage, current, or frequency that causes client equipment to malfunction or fail [38].

> ➤ Power quality is the idea of grounding and powering sensitive equipment in a way that is compatible with the premise wiring system and other connected equipment, as well as appropriate for the device's intended use [40].

On the other side, power quality is defined as "compliance with specified voltage tolerances and voltage ripple" in the IEEE recommended practice Std1709, which deals with medium-voltage DC (MVDC) distribution systems between 1 and 35 kV [40]. That concept essentially reduces power quality to voltage quality, which is essential to DC power distribution systems because DC voltage provides a distributed indicator of power balance in these systems.

I.6.2 DC Power Quality Issues

Power quality issues affect electrical systems' performance and can be classified by their nature and duration. Transients, either impulsive or oscillatory, are short-lived disturbances. Short-duration variations include sags, swells, and interruptions, while long-duration variations involve under voltages, over voltages, and sustained interruptions. Voltage and current imbalances, waveform distortions (e.g., AC offsets, inter-harmonics, noise, notching), and voltage fluctuations further degrade power quality. In the under voltage case, the currents increase to distribute the same amount of energy. This is the effect of incremental negative impedance, due to constant power loads (CPLs). The issues are summarized in the accompanying table.

Table I. 2. DC power quality issues

Class	Indicators	Sources of problems	Effects
Transients: Impulsive	Rise time Fall time Peak magnitude	Lightning strikes Inductance switching	Voltage resonances Insulation breakdown
Transients: Oscillatory	Duration Peak magnitude Spectral content	Line switching Capacitor switching Power variations	Voltage resonances Insulation breakdown
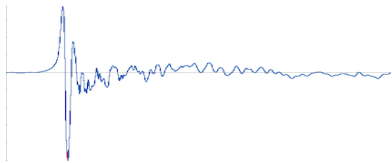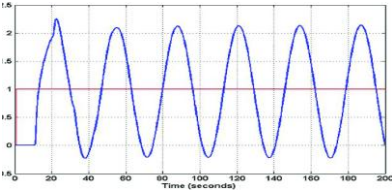
Short duration variation: sag	Duration Magnitude	Capacitor switching Power variations	Equipment shut-down
Short duration variation: swell	Duration Magnitude	Faults Capacitor switching Power variations	Protection malfunction Overstressing equipment Insulation breakdown
Short duration variation: interruption	Duration Magnitude	Faults	Equipment shut-down
Long duration variation: under voltage	Magnitude	Poor system voltage regulation Overloading	Increased losses Voltage instability
Long duration variation: over voltage	Magnitude	Poor system voltage regulation	Overstressing equipment
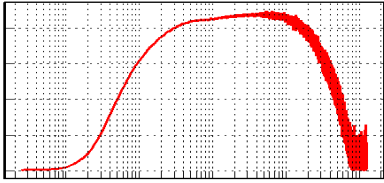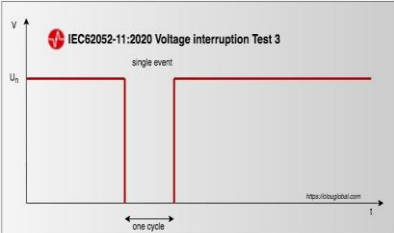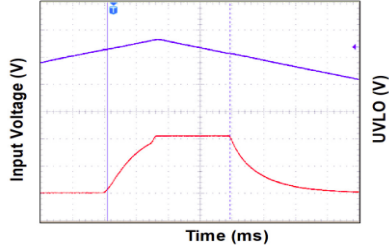
Long duration variation: Interruption	Magnitude	Faults	Equipment shut-down
Imbalance: voltage	Magnitude	Single-pole devices Pole-neutral faults	Pole-neutral overvoltage or undervoltage
Imbalance: current	Magnitude	Single-pole devices	Neutral conductor overloading Increased losses Voltage imbalance
Waveform distortion: AC offset	Magnitude	Faults interconnecting AC and DC system	Increased losses due to reactive currents Voltage sags and swells
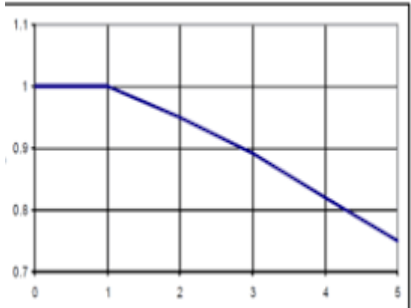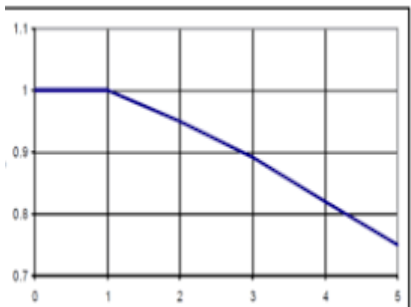
		Electromagnetic coupling	
Waveform distortion: Interharmonics	Spectral content	Switch-mode power converters	Increased losses Increased currents in the filter capacitors Disturbance of measurement and communication devices
Waveform distortion: Noise	Spectral content	Switch-mode power converters PLC communication	Increased losses Increased currents in the filter capacitors Disturbance of measurement and communication devices
Waveform distortion: Notching	Magnitude (notch depth)	Switch-mode power converters	Increased losses Increased currents in the filter capacitors Disturbance of measurement and communication devices
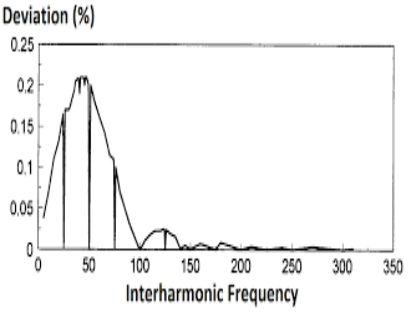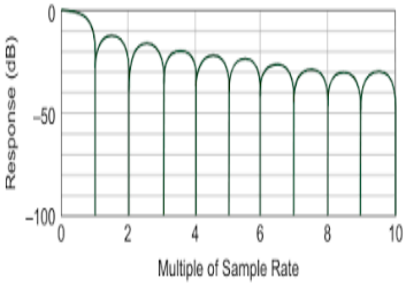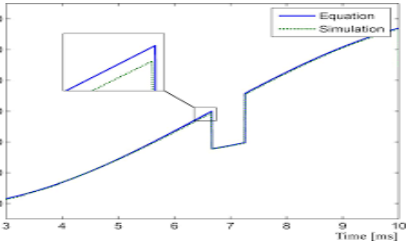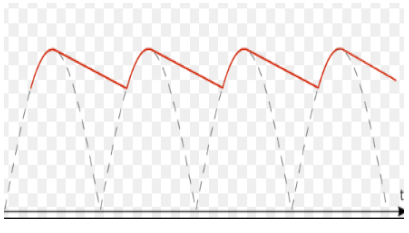
Voltage fluctuations	Spectral content Duration	Low-frequency power oscillations	Light intensity fluctuations Periodic voltage sags and swells

I.6.3   Constant Power Loads (CPLs)

The issue of how two electrical systems interact in a cascade is well-known, and numerous studies have been done to explain this phenomenon for cascaded dc/dc converters and their input filters, as well as for motor drive systems that receive power from a dc power source through inverters and their input filters [41].

Multi-converter power electronic systems are essential for supplying different forms of power and voltage to electrical networks. These systems consist of several power electronic devices configured in different arrangements, such as cascaded systems. In cascaded systems, a source converter regulates the voltage, while a secondary converter adjusts the line voltage for individual loads. Load converters in multi-converter systems behave like constant power loads when they are tightly controlled, maintaining a constant output power despite current variations. Examples of constant power loads include motor drives and electronics with regulated controllers, as well as DC-DC converters [42]

A CPL is a power electronic converter that is strictly regulated. A CPL tends to destabilize its feeder system and displays negative incremental impedance. Figure 11 displays the V-I parameters of a typical CPL. Tightly-regulated dc/dc converters with resistive loads and dc/ac inverter drives are two basic instances of CPL in a dc system. As seen in Figure I. 11, a CPL may manifest itself in four different configurations, each of which could destabilize the feeder system. The current drawn by a CPL increases or decreases in response to changes in the input voltage, as shown in Figure 12 [43].
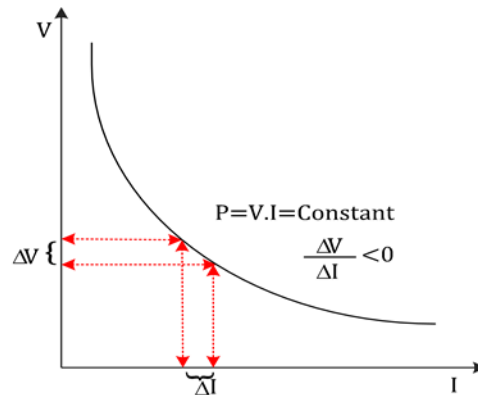
Figure I. 12. *V-I* parameters of a typical CPL

I.6.4   Power Quality Indicators

When defining PQ indicators for LVDC microgrids, it makes sense to use indices that are expressed as ratios of two quantities: the lower quantity represents the average of the DC component of the signal being monitored, and the upper quantity represents the disturbance from the desired/ideal signal. Such indicators are recognizable by their various forms and recollections of the noise-to-signal ratios [44].

I.6.4.1   PQ Indicators in Time Domain

Calculating certain parameters is necessary [44]:

➢ The average DC component

➢ The median of the samples

➢ The percentile variation: This parameter seeks to express how far one side (up or down from the mid-point or the ideal desired DC signal) deviates from the midpoint in terms of percentage from the total number of samples.

➢ The peak-to-peak variation

➢ The RMS variation from the mean

➢ The percentile displacement factor

➢ The RMS variation displacement factor

➢ The combined RMS displacement factor

I.6.4.2   PQ Indicators in Frequency Domain

➢ Calculate the DFT (discrete Fourier transform) of the signal on each Ta_0 , and on each Tw. Indeed a DFT is always associated with spectral leakage. The duration of Ta_0 was chosen

26

in order to preserve compatibility with the approach indicated in the most recent IEC 61000-4-30 Standard [44].

➢ Choose the frequencies where magnitudes are higher than a threshold of 30 % from the maximum amplitude observed in the FFT, and construct the corresponding bandwidths [44].

➢ Calculate the overall distortion factor [44].

I.6.5   Standardizations

I.6.5.1   Transients

Various standards address transients in power systems with specific definitions and classifications. IEEE Std1159 categorizes transients by frequency range: low (<5 kHz), medium (5–500 kHz), and high (0.5–5 MHz). EN50160 defines transient overvoltage as short, highly damped oscillatory or non-oscillatory events lasting milliseconds or less. IEC61000 describes transients as short-duration variations between two stable states.

I.6.5.2   Short and Long Duration Variation

IEEE Std 1159: This standard is used to define and categorize voltage variations according to their duration, magnitude and direction of change. It provides definitions for:

Voltage sag: Voltage drop to 0.1–0.9 pu for short-term (0.5 cycles to 1 min) or below 0.1 pu for long-term (under-voltage).

Voltage swell: Voltage rise above 1.1 pu for short-term or prolonged (overvoltage).

Interruption: Voltage below 0.1 pu for short-term or complete voltage loss for long-term.

IEC 61000: This standard offers broader definitions of voltage variations:

Voltage dip: Synonymous with sag; temporary voltage reduction.

Voltage swell: Temporary voltage increase above a threshold.

Interruption: Similar to a voltage dip but with a lower threshold.

I.6.5.3   Imbalance

IEEE Std 1159: Defines voltage imbalance using the voltage unbalance factor (VUF), calculated as the ratio of negative or zero-sequence voltage to positive-sequence voltage, and specifies a limit of 3%.

EN 50160: Uses the same VUF definition but imposes a stricter limit of 2% for voltage imbalance.

IEC 61000: Adopts the same definition as IEEE Std 1159, aligning with the 3% limit.

I.6.5.4   Waveform Distortion

IEC 61000 series:

IEC 61000-2-2: Addresses harmonic voltage distortion in low-voltage (LV) systems (<1 kV, currents <16 A) with a Total Harmonic Voltage Distortion (THDv) limit of 8% for long-term effects.

IEC 61000-3-4: Sets limits for harmonic current distortion in LV electrical systems (<1 kV) with currents below 16 A.

IEEE 519-1992: Focuses on systems with voltages between 120 V and 6.9 kV, specifying a THD voltage limit of 5% for the AC bus. It also defines current distortion limits based on system parameters like voltage and short-circuit capacity.

IEC 61000-2-2 emphasizes harmonic distortion in LV systems with smaller currents, while IEEE 519-1992 targets higher voltage systems and includes detailed current distortion limits based on system characteristics.

The THD limit for voltage is stricter in IEEE 519-1992 (5%) compared to IEC 61000-2-2 (8%).

I.6.5.5   Voltage Fluctuations

IEC 61000-3-3 and IEC 61000-3-11 define the limits of voltage fluctuations caused by electrical equipment in low-voltage networks (<1 kV). IEC 61000-4-15 provides methods for measuring flicker intensity, enabling indirect assessment of voltage stability.

28

I.7   Control Methods for DC-DC Converters

I.7.1   Study of Classical and Advanced Control Techniques

Due to the non-linearity and time-dependency of converter operation, and the incremental negative impedance effects of constant-power loads, conventional linear control methods have their limitations. Consequently, non-linear control methods have to be applied. Techniques to compensate for CPL instability can be achieved by adding an extra element, such as passive elements or devices, to the electrical system, or by modifying the control loop of a source or load converter [3].
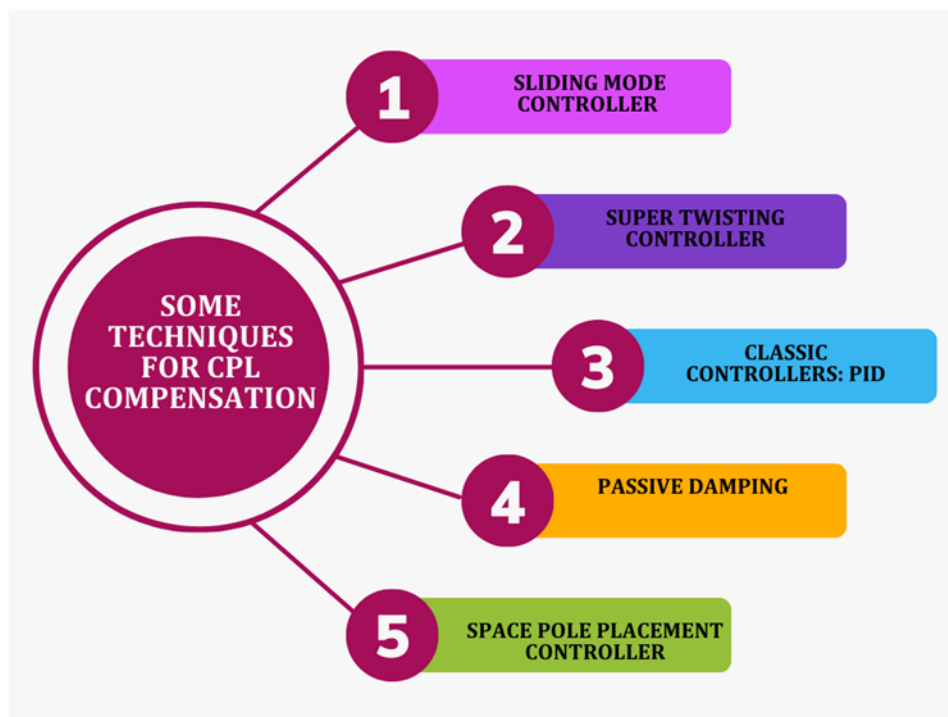
Figure I. 13. Some techniques for CPL compensation

I.7.1.1   Passive Damping

 Using this method, the system damping is raised by introducing passive components (resistances, resistance-capacitance, and resistance-inductance) to the system under consideration in order to compensate for the negative incremental impedance effect of the CPLs. The system becomes larger, heavier, and more expensive as a result of this method. Additionally, the efficiency of the

29

system is negatively impacted by passive components since they cause high power dissipation, especially when resistance is utilized in tandem with a filter capacitor [43].

I.7.1.2   Sliding Mode Controller

In order to guarantee stability under parameter constraints, sliding mode control has been carefully investigated for nonlinear robust control [45].

The sliding mode control is one of the variable structure controls that aims to obtain an independent dynamic of the system, particularly its likely closed-loop oscillations. Three primary phases that are highly dependent upon one another can be taken to complete the design of the control system [46]:

> ➢ Surface selection
> ➢ Establishment of the conditions of existence of the convergence.
> ➢ Determination of the control law.

I.7.1.3   Super Twisting Controller

One of the strongest 2-order continuous SMCs is the super-twisting algorithm (STA), which guarantees both chattering reduction and all essential characteristics of its conventional 1-order form [47]. Regardless of changes in load or disturbances to the input voltage, this control reduces the initial current peak and regulates the output voltage [48]. The derivatives of the sliding variable are not necessary to be known by a super-twisting sliding mode controller [49].

I.7.1.4   Space Pole Placement Controller

Determining the system's poles to satisfy design requirements is the fundamental concept of state space pole placement control. We can move the system transfer function poles to a new pole location that satisfies a design requirement if they are not in the ideal location. Furthermore, it is possible to stabilize unstable systems in addition to making desired system responses [50].

I.7.1.5   PID Controller

A PID controller measures the DC microgrid's output voltage and compares it to a desired reference voltage. It then adjusts the control signal (e.g., pulse-width modulation for a DC-DC converter) based on the proportional, integral, and derivative terms of the error (difference between reference and actual voltage). This helps regulate the voltage despite the CPL's tendency to draw constant power regardless of voltage fluctuations.

I.8 Literature Review

I.8.1 Passive Damping Techniques to Compensate For the Destabilizing Effect of CPLs

In the context of passive damping techniques, A method called inductor core biasing technique (ICBT) can reduce current ripple in DC-DC converters without increasing inductance value [5]. It has been proven that the suggested ICBT can substantially decrease the necessary inductance value to attain the same ripple current while enhancing saturation capability and efficiency for a given core size. However, it should be noted that this approach requires an additional circuit, which may increase the expenses and dimensions of the overall setup.

An effective solution for replacing large capacitors in DC systems using a bidirectional buck-boost converter and an additional capacitor designed to eliminate ripples in [6]. The approach recommends three control techniques for regulating the voltage of the supplementary capacitor. This method can operate seamlessly under a broad range of operating conditions, but it should be noted that it employs a relatively intricate circuit.

A recent study, presents a novel design approach that prioritizes voltage stability and minimizes electrical current surges in cascaded buck converters. The proposed method involves identifying the most suitable combination of output filter parameters for load converters and the main DC bus voltage. With just a few initial parameters and an optimization process, designers can determine the final values for bus voltage and output filter parameters for converter one. Additionally, this approach allows for the evaluation of each variable's impact and facilitates selecting the optimal balance between stability and short-circuit energy. However, energy dissipation remains a challenge for this study and other similar research endeavors, as it tends to reduce efficiency [7].

A zero-ripple boost cell and a coupled inductor are combined to create a high output voltage step-up in a high boost ratio non-isolated converter with a ripple-free input current. The resonance of the linked inductor's leakage inductance and the switch's parasitic capacitance results in a voltage spike that is suppressed by a passive snubber. Consequently, the efficiency of the converter can be raised by using a low-voltage rated metal oxide semiconductor field effect transistor (MOSFET) with a low rDS(ON). Furthermore, it is possible to achieve an input current that is free from ripples, which simplifies the electromagnetic interference (EMI) filter. The analysis results of the suggested converter are confirmed by the experimental results of a 100 W (40 V/200 V) prototype [51].

I.8.2   New Converters Topologies to Compensate for the Destabilizing Effect of CPLs

The second suggested strategy uses novel DC-DC converter topologies [52] proposes a new DC-DC converter topology consisting of a low-volume DC-DC step-up converter operating in parallel with a switched capacitor voltage multiplier (SCVM). This structure allows a voltage gain of four times with reduced current ripple. In addition, the recommended converter might be more suitable for high-power applications. However, the problem with this method is the use of a large number of diodes and transistors. The addition of passive components to the circuit and the use of a higher number of switches increase:

- ➢ The overall cost;
- ➢ The size and complexity of the circuit;
- ➢ Switching and conduction losses;

A zero-ripple boost cell and a coupled inductor are combined to create a high output voltage step-up in a high boost ratio non-isolated converter with a ripple-free input current. The resonance of the linked inductor's leakage inductance and the switch's parasitic capacitance results in a voltage spike that is suppressed by a passive snubber. As a result, employing a low-voltagerated metal oxide semiconductor field effect transistor (MOSFET) with a low rDS(ON) can increase the converter's efficiency. Moreover, a ripple-free input current can be obtained, which makes the electromagnetic interference (EMI) filter easier to use. The experimental results of a 100 W (40 V/200 V) prototype verify the analysis results of the proposed converter [53].

Researchers are developing a new high-voltage gain DC-DC boost converter to enhance Maximum Power Point Tracking (MPPT) systems for photovoltaic (PV) panels. This converter, utilized alongside an MPPT boost converter, addresses issues like insufficient voltage supply and voltage stress across power switches. By minimizing input current source ripples and boosting voltage gain, the proposed converter aims to improve efficiency and prolong the lifespan of PV panels and semiconductor devices. Hardware tests on a laboratory prototype confirm the converter's effectiveness under varying weather conditions [10].

The work in [11] focuses on a boost converter that is magnetically coupled-inductor SIDO (CI-SIDO). Reduced input current ripples in any converter are necessary to meet stringent input current ripple regulations, lessen the need for input filters, and provide a number of other advantages. By altering gate pulses, maximum ripple cancellations are added to converters such as interleaved

boost in order to lessen input current ripples. On the other hand, the CI-SIDO boost has two distinct output voltages and two uneven inductances, in contrast to an interleaved boost. The greatest ripple cancellation in the CI-SIDO boost converter is dependent on the linked inductors' design in addition to the shifting of gate pulses.

I.8.3   *Active Damping Techniques to Compensate for the Destabilizing Effect of CPLs*

Passive damping methods have power dissipation issues that can be avoided by opting for active damping methods. The effect of phase shift is analyzed in [8] between duty cycles of two-stage cascaded converters, and it was found that a proper adjustment in the phase shift can reduce the RMS current ripple of the capacitor without affecting the normal converter operation or requiring additional sensing circuits. Besides, it leads to an overall efficiency improvement. However, the control flowchart used to regulate the phase shift between the duty cycles of the two power stage converter switches can be complex.

The work in [9] addresses current ripple reduction in power systems by analyzing its main sources and proposing mitigation methods. It identifies two key sources: 100-Hz bus voltage ripple and quantized error-induced ripple from low pulse-width modulation resolution. To address these, the paper develops a small-signal model for DC/DC converters and introduces PIDR control and HRPWM technology. Experiments with a 2-kW bidirectional DC/DC converter prototype show an 81.5% reduction in current ripple at full load using these methods.

A new technique has been proposed in [54] for controlling both uniform and non-uniform DC-DC systems that are connected in parallel. This fully decentralized controller uses a gradient descent technique to minimize the fundamental switching harmonic in the current and voltage ripple. The algorithm is implemented in each converter by adjusting the PWM phase shift based on the local terminal voltage sampled at each switching cycle. One major advantage of this approach is its simplified digital implementation that does not require complex optimization algorithms, look-up tables, high-fidelity detection, or oversampling measurements. However, it is important to note that the use of sensors in this method may be costly, especially if they are highly precise or specialized.

In [55] a strategy for reducing the inductance current ripple of a DC-DC converter in a two-stage power conversion system made up of an interleaved three-level multiphase DC-DC converter and a grid-connected PWM converter is proposed. The three-stage DC-DC converter is set up in

parallel and runs in interleaved mode to lessen output voltage ripple. On the other hand, a circulating current brought on by the interleaved operation raises each DC-DC converter's inductor current ripple, which causes inductor saturation and system loss. The three-phase, three-level interleaved DC-DC converter's inductor and output current ripple are mathematically analyzed in this study, and the impact of the DC-DC converter's output voltage and duty ratio on each current's ripple is discussed. This analysis forms the basis of a proposed strategy that uses the PWM converter to regulate the optimal DC link voltage in order to minimize the ripple in the inductor current while using the duty ratio to control the DC-DC converter.

A discrete-state feedback controller combining D-stability theory and the GA technique has been proposed and experimentally validated in [56]. The proposed GA technique is used to search for the optimal closed-loop eigenvalues to obtain the desired response of the closed-loop LED driver subject to a proposed cost function equation. The experimental results of the proposed methodology demonstrate that the discrete controller designed using GA can ensure good performance of the reference controller with low error between reference and inductor current, as well as low overshoot and good performance of the tracking controller.

I.9 Conclusion

An overview of dc microgrids, dc-dc converters, and the power quality of these grids is given in brief in this chapter. In order to minimize current ripples in dc-dc converters, numerous techniques have already been developed. By evaluating these techniques' efficacy, complexity, and applicability for usage in DC microgrids, we show the importance of our study. Three methods of controlling DC microgrids using cascading dc-dc converters are thoroughly compared in the next chapter.

Chapter 2: A Comparative Study of Three Methods for Controlling Cascaded Systems in DC Microgrids

II.1 Introduction

Before introducing the novel control technique proposed in our work, a comparative study was conducted to evaluate the performance of three different control methods for load converters. These methods were evaluated in terms of their ability to handle constant power loads and their impact on system stability and power quality. A basic structure of a DC microgrid is proposed in this chapter, comprising two cascaded boost converters. A cascaded PI regulator is used for the source-side converter, which is controlled in current and voltage. The load-side converter is controlled by three variants;

A cascaded PI regulator

Sliding mode control

Super twisting control

II.2 A Comparative Study of Three Methods for Controlling Cascaded Systems in DC Microgrids

The choice of a cascaded boost converter, which essentially consists of two or more boost converters connected in cascade, allows a much greater increase in voltage to be achieved than with a single stage. This is useful in applications where it is necessary to take a low input voltage and increase it significantly. In the under voltage case, the currents increase to distribute the same amount of energy. This is the effect of incremental negative impedance, due to constant power loads (CPLs). This destabilizing effect is caused by the extensive interconnection of the power electronic converters [57].

A basic DC microgrid structure, which is faithful to the general model, and which allows to take into account all the constraints that can be found in a real system, is proposed in this study, consisting of two cascaded Boost choppers supplied by a DC voltage source, as shown in Figure II. 1. The main goal of this research is to compensate for the load converter's destabilizing effect without affecting the supply converter's performance. A cascaded PI regulator controls the supply converter's voltage and current, while the load converter's voltage and current are controlled by three different techniques under input voltage changes. The first method uses two cascaded PI

regulators and the second one, the output voltage will be controlled by the current control by a sliding mode controller, and the last method, is to control the output voltage by a PI regulator and the inductor current by the super twisting control. The three control methods are simple, but each control has advantages and disadvantages. The classic PI cascade controller is both fast and efficient. The SMC controller is the fastest, but it has a high current ripple rate and instabilities in transients. The last controller, allows to have a minimal current ripple, but its dynamics is slow compared to the two other control methods.

II.2.1 Proposed Structure and its Control

A DC microgrid structure consisting of two cascaded DC-DC Boost converters fed by a battery is described in this section, as seen in figure II. 1. The source-side converter is controlled by a cascaded PI controller. Three current and voltage control methods will be used for the load converter.
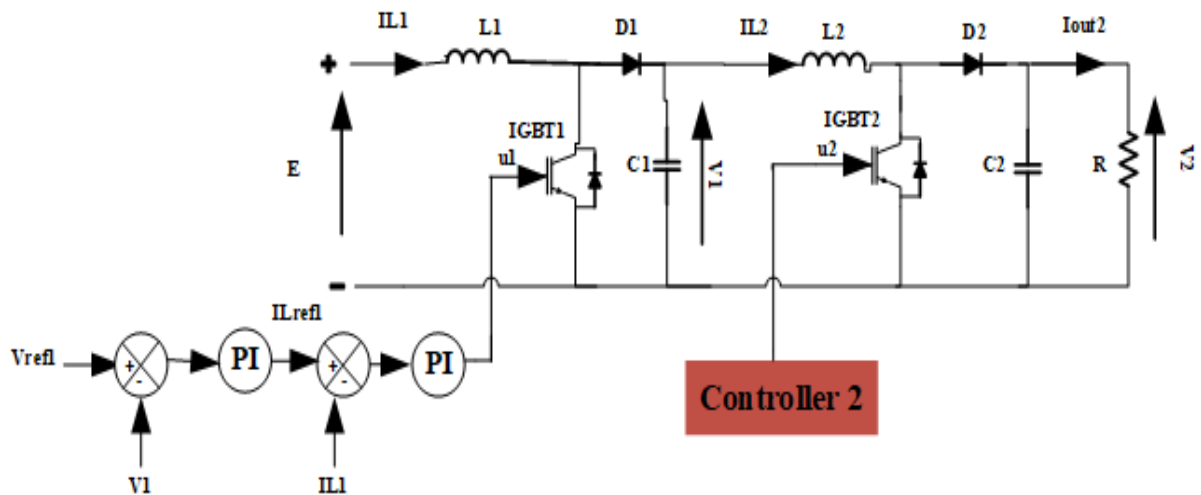
Figure II. 1. System under study

The conventional boost converter was chosen over other converter topologies for two main reasons: its low component number and its simplicity of control [58].

The control of the output voltage and inductor current of the source converter is performed using two cascaded PI regulators where the inner loop is designed to be much faster than the outer loop.

While, for the control of the load converter, we will apply three different control methods: PI in cascade, SMC and PI-STC in cascade under input voltage variation.

The dynamic model of the supply converter is given by equations (1) and (2):

$$\frac{dI_{L1}}{dt} = -(1 - u_1)\frac{1}{L1}V_1 + \frac{E}{L1} \qquad (1)$$

$$\frac{dV_1}{dt} = (1 - u_1)\frac{1}{C1}I_{L1} - \frac{I_{L2}}{C1} \qquad (2)$$

The transfer functions of the voltage and current regulators are respectively given by equations (3) and (4):

$$G_{V1}(s) = K_{pv1} + \frac{K_{iv1}}{s} \qquad (3)$$

$$G_{I1}(s) = K_{pi1} + \frac{K_{ii1}}{s} \qquad (4)$$

II.2.1.1 Cascaded PI Controllers

The dynamic model of the load converter is given by equations (5) and (6):

$$\frac{dI_{L2}}{dt} = -(1 - u_2)\frac{1}{L2}V_2 + \frac{V_1}{L2} \qquad (5)$$

$$\frac{dV_2}{dt} = (1 - u_2)\frac{1}{C2}I_{L2} - \frac{V_2}{RC2} \qquad (6)$$

The control of the DC-DC load converter consists in integrating the current loop in cascade with the voltage loop. The correctors used are of the Proportional-Integral PI type. The expressions of the current and voltage PI regulators are respectively given by (7) and (8):

$$G_{V2}(s) = K_{pv2} + \frac{K_{iv2}}{s} \qquad (7)$$

$$G_{I2}(s) = K_{pi2} + \frac{K_{ii2}}{s} \qquad (8)$$

II.2.1.2 Sliding Mode Controller (SMC)

Among the variable structure controls, we find the sliding mode control [59, 60], which aims to get an independent dynamic of the system, especially its probable oscillations in closed loop [61]. The

design of the control system can be achieved in three main steps that are strongly dependent on each other:

Surface selection

$$\begin{cases} s = I_{L2} - I_{Lref2} \\ \quad \text{with} \\ I_{Lref2} = \frac{V_{ref2}{}^2}{RV_1} \end{cases} \tag{9}$$

Establishment of the conditions of existence of the convergence.

Determination of the control law.

The control law of the load converter is:

$$u_2 = 1 - \frac{V_1}{V_2} + \frac{1 - sign(s)}{2} \tag{10}$$

II.2.1.3 Cascaded PI-*super Twisting Controller (STC)*

The Super Twisting control is a control that offers all the fundamental qualities of traditional first-order sliding mode control, as well as the reduction of oscillations. In other words, it is not only robust to system uncertainties and external disturbances, but it can also follow the system with high precision. Unlike second-order sliding mode algorithms, super twisting control requires only knowledge of the sliding variable and not its time derivative [62]. The control law can be written as follows:

$$u_2 = 1 - \frac{V_1}{V_2} - \lambda. \left| I_{L2} - I_{Lref2} \right|^{0.5}. sign\left(I_{L2} - I_{Lref2}\right) - \int \gamma. sign\left(I_{L2} - I_{Lref2}\right) \tag{11}$$

I_{Lref2} is obtained by the PI controller.

Where λ and γ are designed parameters. They can be obtained using the sufficient conditions that are required to ensure the convergence:

$$\lambda > \sqrt{\frac{2 * (\text{Гm} * \gamma + \Phi)^2}{\text{Гm}^2 * (\text{Гm} * \gamma - \Phi)}}$$

$$\gamma > \frac{\Phi}{\text{r} m}$$

II.2.2 Simulation Results of the Studied Chain under Input Voltage Variation

The parameters of the two dc-dc converters used in this work are presented in the table II. 1. From 0 to 1 second and 2 to 3 seconds, the input voltage is 24 volts, and from 1 to 2 seconds, it is 35 volts.

Table II. 1. Circuit parameters

Circuit parameters	Value
Input voltage, $E(V)$	24 then 35
Inductors, $L = L_1 = L_2(mH)$	1
Capacitors, $C = C_1 = C_2(\mu F)$	470
Load resistor, $R\ (\Omega)$	15
Switching frequency of the feeder converter, $f_{d1}(KHz)$	20
Switching frequency of the load converter, $f_{d2}(KHz)$	10
Desired output voltage of the feeder converter, $v_{ref1}(V)$	45
Desired output voltage of the load converter, $v_{ref2}(V)$	100

The PI controllers allow the output voltages of the supply and load converter to converge rapidly and smoothly to the desired values, although their responses have overshoots of 44.44 % and 18 %, respectively, as shown in figure II. 2. The output voltages also show overshoots when the input voltage varies, but they rapidly return to the steady state. The input and output currents of the load converter, illustrated in figures II. 3 and 4, show sudden changes when the input voltage varies, but they quickly return to the steady state. The inductor current's ripple factor remains constant throughout the three-time phases. Figure II. 5 depicts the total system's efficiency. When the entire system's input voltage is increased, it gets a little higher.
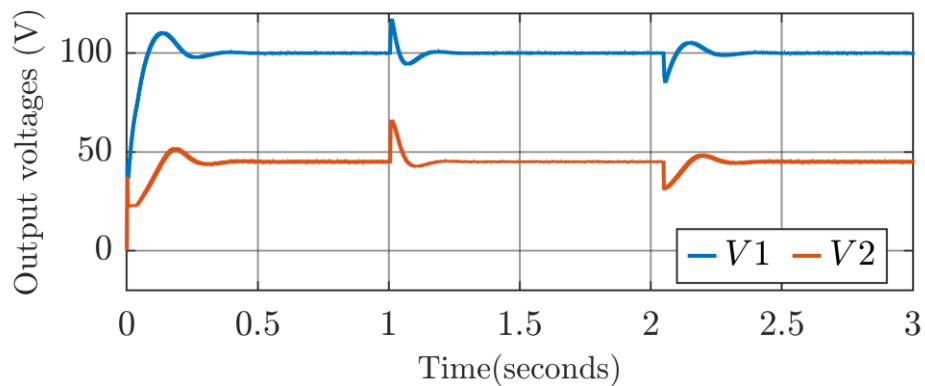
Figure II. 2. Measured output voltages using cascaded PI regulators
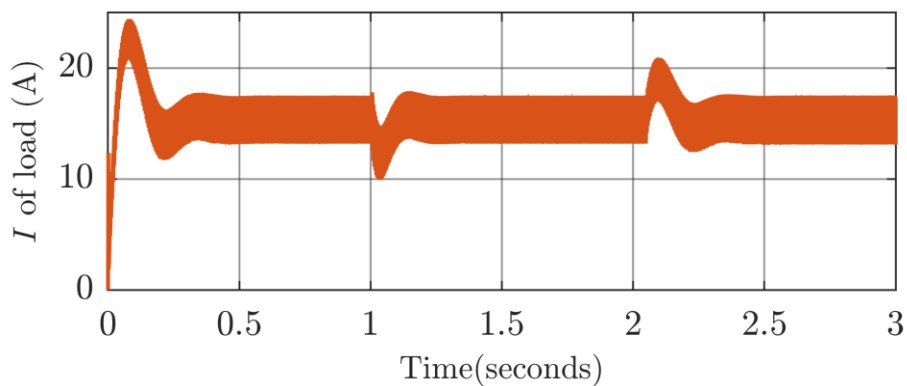
Figure II. 3. The load converter's inductor current using cascaded PI regulators
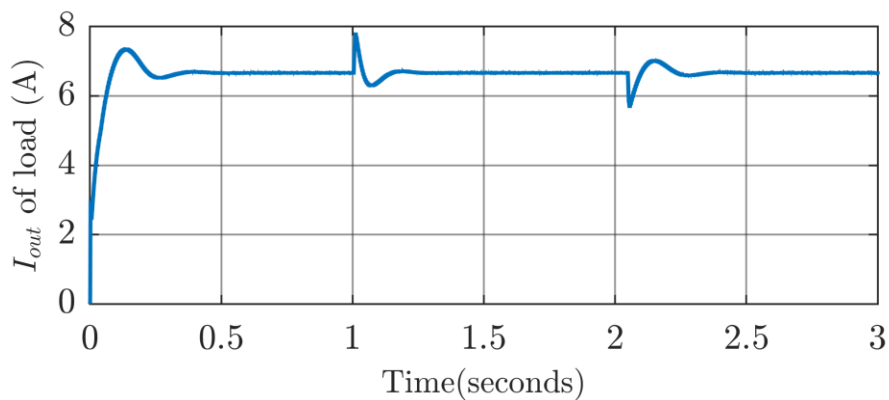
Figure II. 4. Output current of the load converter using cascaded PI regulators
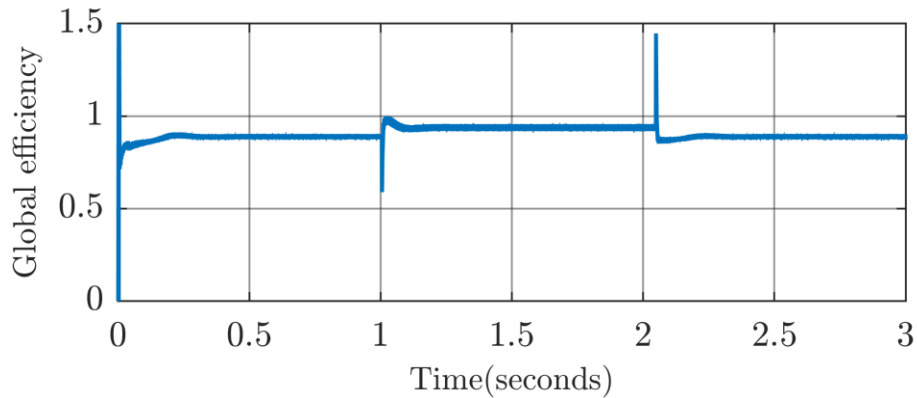
Figure II. 5. Total system efficiency using cascaded PI regulators

When the sliding mode control is applied, we can observe on figure II. 6 that when we feed the system with a 24 V input voltage at t=0 s and t=2s, severe unstable fluctuations appear on the output voltages of the two choppers, and after that the responses stabilize. Overshoots about 73.33 % and 17 % appear in the output voltage responses of the source converter and load, respectively, at time t=1s or when an input voltage of 35 V is applied. The inductor current of the load converter is shown in figure II. 7 and the output current of the load converter is shown in figure II. 8. The ripple of the inductor current decreases as the input voltage rises from 24 V to 35 V. With rising input voltage, the average value of overall system efficiency, as illustrated in figure II. 9, improves.
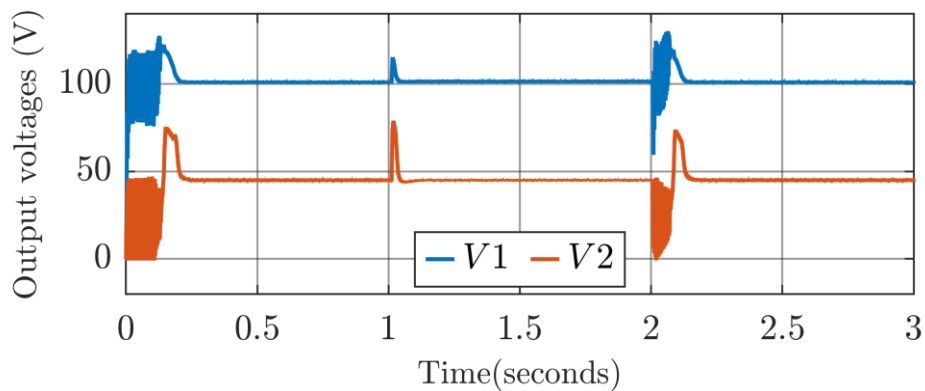
Figure II. 6. Measured output voltages using SMC
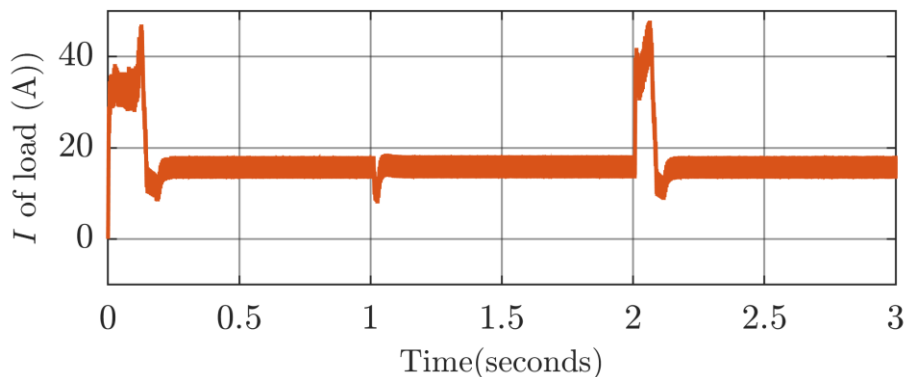
Figure II. 7. Load converter's inductor current using a SMC controller
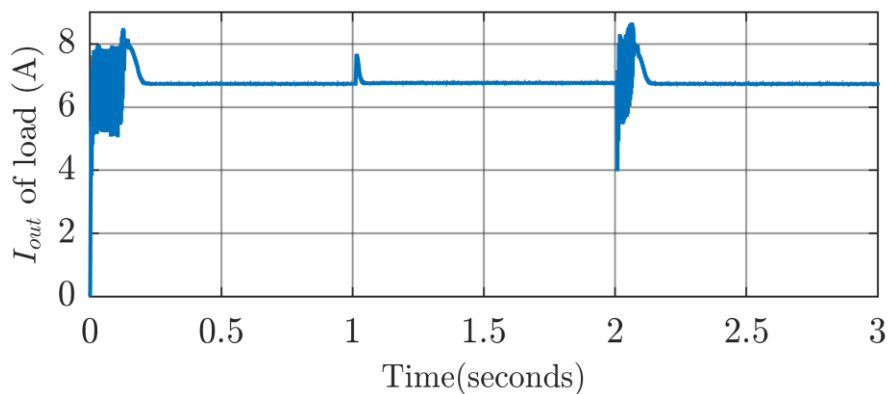
Figure II. 8. Load converter's output current using a SMC controller
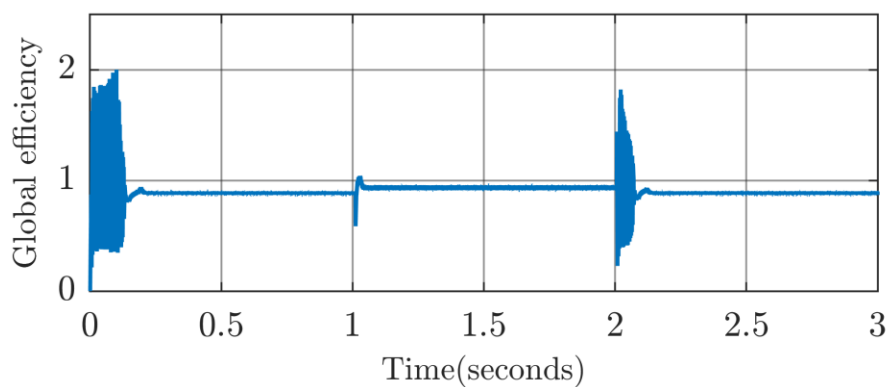
Figure II. 9. Average efficiency value of the overall system using SMC controller

Figure II. 10 depicts the measured voltages of the two cascaded converters. The super twisting control, as illustrated in this figure, is able to cancel the severe unstable voltage fluctuations found with the sliding mode control. When a 35V input voltage is provided at time t=1s, a swell appears. When a 24V input voltage is provided at time t=2s, a sag appears. Figures II. 11 and 12 show the load converter's inductor and output currents, respectively. After raising the input voltage, there is a slight decrease in the inductor current ripple factor. The average value of the overall system efficiency is shown in figure II. 13. As in the previous cases, the efficiency becomes a little higher with increasing input voltage.
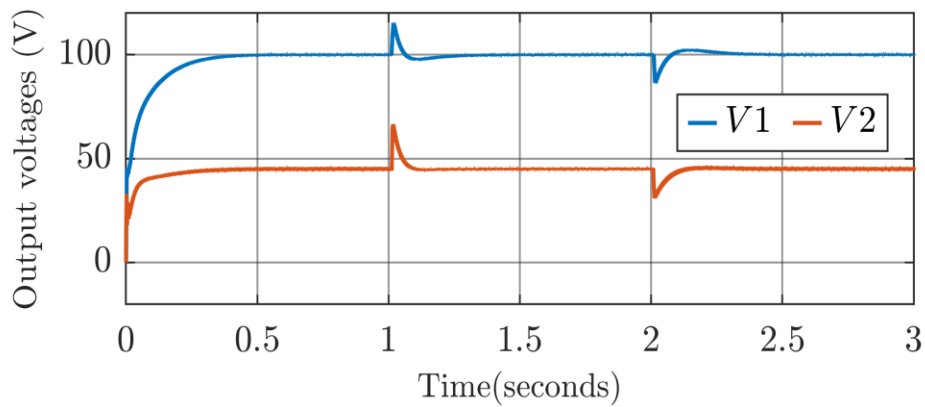
Figure II. 10. Measured output voltages using cascaded PI-super twisting controllers
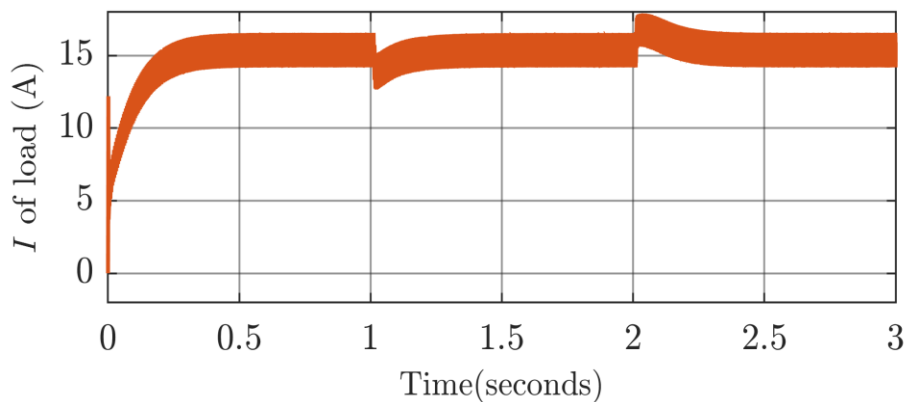
Figure II. 11. Inductor current of the load converter using cascaded PI-super twisting controllers
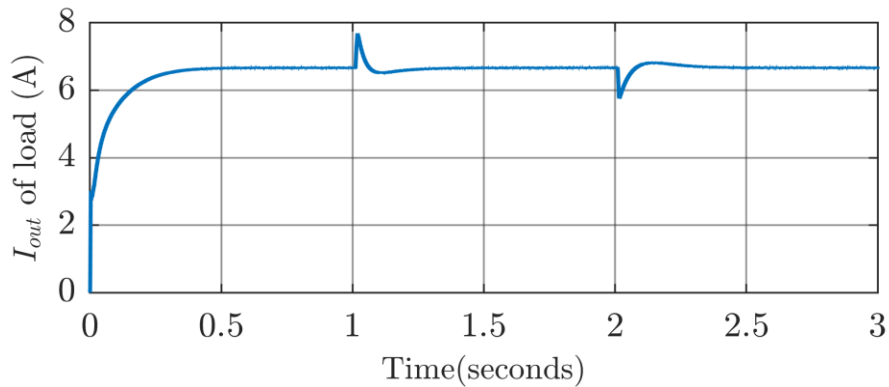
Figure II. 12. Output current of the load converter using cascaded PI-super twisting controllers
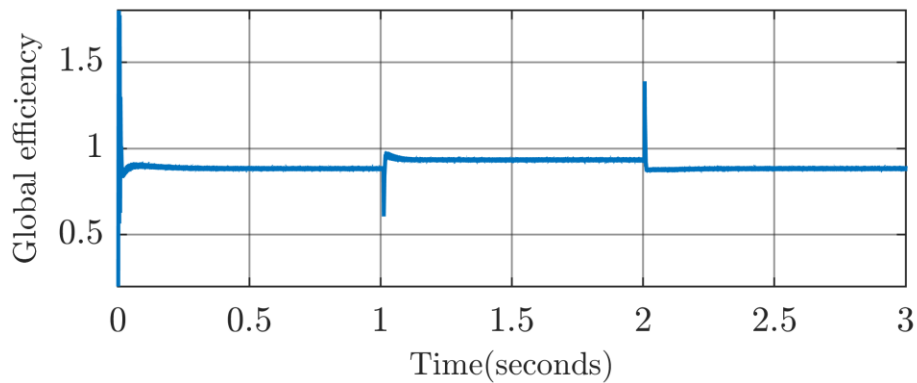
Figure II. 13. Average efficiency value of the overall system using cascaded PI-super twisting controllers

Based on the simulation results of the three control methods, it is noted that, the super twisting control allows having a more stable response with a minimum ripple factor of the inductor current, unlike the results of the sliding mode control. The disadvantage of this control method is that it is slow and has a slightly lower efficiency compared to the other two controls. A comparison of the performances of the three control methods is summarized in the following table II. 2.

Table II. 2. Summarizes the results of the three control methods:

	rapidity	Ripple factor of the inductor current		Efficiency	
		24 V	35 V	24 V	35 V
Cascaded PI	fast	27.64%		88.85%	95.7%
SMC	faster	34.75%	34.18%	88.7%	93.45%
Cascaded PI-STC	little slow	15.42%	15.18%	88.25%	93.25%

II.3 Conclusion

In this work, a basic DC microgrid structure is studied, three control methods have been realized under the variation of the input voltage of the global system in order to compensate the destabilizing effect of constant power loads. The simulation results of the cascade PI controller showed that this type of control guarantees a good accuracy with a high efficiency. For the system controlled by the sliding mode, severe unstable fluctuations of voltage and current have been appeared but it improves the speed of the system compared to the first controller. The super twisting controller guarantees good accuracy and stability with less ripple factor of the load converter inductor current (CPL), the disadvantage of this control is that it is a bit slow compared to the other two types of control.

CHAPTER 3: Design of an Advanced Control Strategy for the Minimization of Current Ripples in Cascaded DC-DC Converters

III.1 Introduction

The cascaded DC-DC converter is the master element of the DC microgrid, connecting multiple DC-DC converters via a common bus, this extensive interconnection causes instability and/or current ripples in the overall system due to the load-side DC-DC converter acting as a constant power load. In this chapter, a method of active current ripple damping is presented. This method takes the fundamental of the inductor current and uses it in super-twist sliding mode control (STSMC).

III.2 Super-Twisting Control and Harmonic Extraction: A Novel Approach to Minimize Input Current Ripples in Cascaded DC-DC Converters

III.2.1 Theoretical Model

This study focuses on mitigating the input current ripple in a cascaded DC-DC converter. The system under study is illustrated in figure III. 1. The system has two conventional DC-DC boosts; the one connected to the DC power source is named the source converter, and the other is the load converter. The two converters are controlled separately and have different switching frequencies.
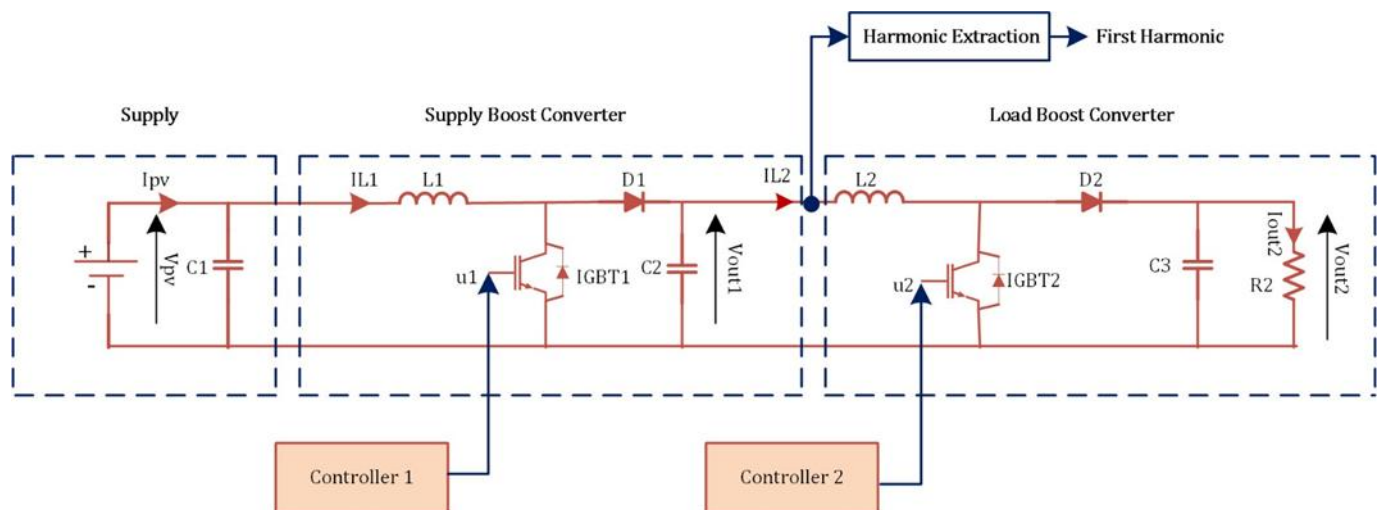
Figure III. 1. Control design of the cascaded boost converter

III.2.1.1 State Space Model of the Cascaded Boost Converter

The state-space model of the cascading boost converters is presented in this sub-section to describe the functionality of both converters and the various variable names used in the following sections [63]:

$$\dot{x_1} = -\frac{(1-u_1).V_{out1}}{L_1} + \frac{V_{in1}}{L_1} \qquad (1)$$

$$\dot{x_2} = \frac{(1-u_1).I_{L1}}{C_1} - \frac{I_{L2}}{C_1} \qquad (2)$$

$$\dot{x_3} = -\frac{(1-u_2).V_{out2}}{L_2} + \frac{V_{out1}}{L_2} \qquad (3)$$

$$\dot{x_4} = \frac{(1-u_2).I_{L2}}{C_2} - \frac{V_{out2}}{C_2 R_2} \qquad (4)$$

With $x_1 = I_{L1}$; $x_2 = V_{out1}$; $x_3 = I_{L2}$ and $x_4 = V_{out2}$.

III.2.1.2 Control Design of the Power Converter

To enhance the generality of our study, a conventional cascaded proportional-integral (PI) controller is employed for the first chopper, as shown in figure III. 2. Compared to a simple PI, implementing a cascaded PI controller enables a more secure and reliable performance of the boost converter. The transfer function from the control input to the power converter output is expressed in the following form [64]:

$$G_{b1}(s) = \frac{G_{d0}.(1-s.\frac{1}{w_z})}{1+s.\frac{1}{Q.w_0}+s^2\frac{1}{w_0^2}} \qquad (5)$$

With $G_{d0} = \frac{V_{out1}}{(1-D_1)}$; $w_z = \frac{R_1}{L_1}.(1-D_1)^2$; $w_0 = \frac{(1-D_1)}{\sqrt{L_1.C_1}}$ and $Q = (1-D_1).R_1.\sqrt{\frac{C_1}{L_1}}$.

49

Where the load converter is considered as a load of the first converter named R_1.

The expressions for the PI voltage and current controllers are given respectively by equations (6) and (7)

$$G_{c1}(s) = G_{cv}.(1 + \frac{W_{Lv}}{s}) \qquad (6)$$

$$G_{c2}(s) = G_{ci}.(1 + \frac{W_{Li}}{s}) \qquad (7)$$

With $K_{pv} = G_{cv}$; $K_{iv} = G_{cv}W_{Lv}$; $K_{pi} = G_{ci}$ and $K_{ii} = G_{ci}W_{Li}$.

The PI controller gains of the source converter are determined by a frequency analysis (Bode diagram).
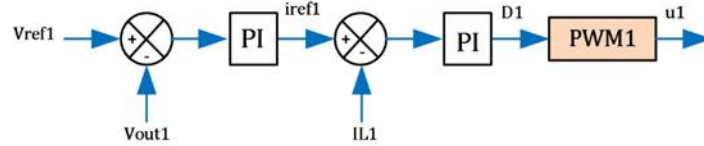
Figure III. 2. Voltage and current control of the DC-DC supply converter

III.2.1.3 Control Design of the Load Converter

The load side converter -which acts as a CPL- is the most fragile part of a DC microgrid. Therefore, a CPL poses a stability challenge that must be handled carefully to guarantee the stability of the whole system. Thus, in this study, we used the super-twisting controller for its robustness.

Besides the robustness, input current ripple is the other concern in this study. Therefore, a new sliding surface is proposed for the super-twisting controller that considerably reduces the input current ripples. Furthermore, a weighted fundamental component is subtracted from the input current; this approach is detailed in the following sub-sections. The control design of the load converter is shown in figure III. 3.
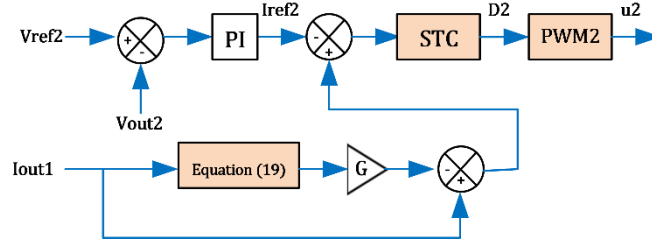
Figure III. 3. Voltage and current control of the DC-DC load converter

III.2.1.4 Fundamental Component Extraction

The input current ripples of the CPL are analyzed in terms of harmonics using a Fourier series decomposition. The inductor current is expressed as follows:

$$\begin{cases} I_{L2} = \dfrac{\Delta I_{L2}}{D_2 T_2} t + I_{min}; 0 < t < D_2 T_2 \\ I_{L2} = \dfrac{-\Delta I_{L2}}{(1-D_2)T_2}(t-T_2) + I_{min}; D_2 T_2 < t < T_2, \end{cases}$$

(8)

According to Fourier series theory, the input current (load converter inductor current or source converter output current), shown in figure III. 4, is decomposed into a DC component and a series of sine and cosine waveforms as follows [64]:
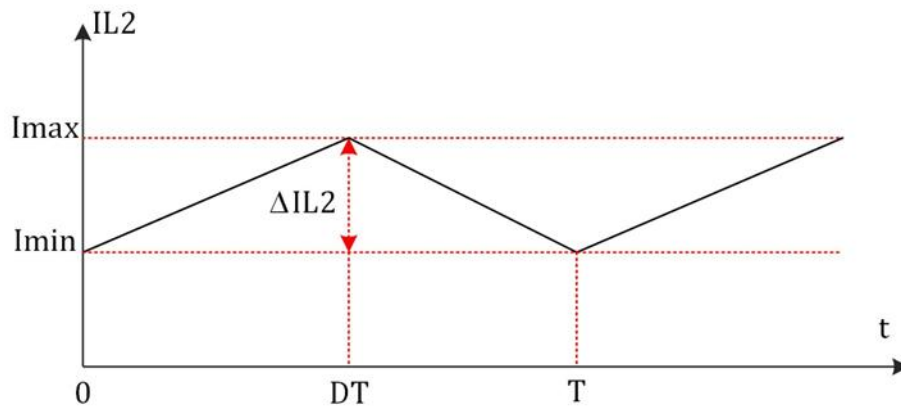
Figure III. 4. Inductor current waveform of the load converter (CPL)

51

$$i_{CPL}(t) = i_{out1}(t) = I_{L2}(t) = \frac{a_0}{2} + \sum_{n=1}^{\infty}(a_n.cos(nwt) + b_n.sin(nwt))$$

(9)

Where $w = \frac{2\pi}{T_2}$, T_2 is the signal period. The coefficients a_n and b_n are:

$$a_n = \frac{2}{T_2}\int_0^T i_{CPL}(t).cos(nwt)dt$$

(10)

$$b_n = \frac{2}{T_2}\int_0^T i_{CPL}(t).sin(nwt)dt$$

(11)

Therefore, the amplitude and phase of the nth harmonic component of the input current is obtained by:

$$A_n = \sqrt{a_n^2 + b_n^2}$$

(12)

$$\varphi_n = \arctan\frac{b_n}{a_n}; a_n > 0$$

(13)

The coefficients a_n and b_n is obtained as:

$$a_0 = 2I_{min}$$

(14)

$$a_n = \frac{1}{D_2(1-D_2)}\frac{1}{n^2}\frac{\Delta I_{L2}}{2\pi^2}(cos(2n\pi d) - 1); n \geq 1$$

(15)

$$b_n = \frac{1}{D_2(1-D_2)}\frac{1}{n^2}\frac{\Delta I_{L2}}{2\pi^2}(sin(2n\pi d)); n \geq 1$$

(16)

The amplitude and phase of nth harmonic components are obtained as follows:

$$A_n = \frac{1}{n^2 \pi^2} \frac{V_{out1}}{L_2 f_{d2}} \frac{1}{(1-D_2)} \sin(n\pi D_2); n \geq 1 \qquad (17)$$

$$\varphi_n = n\pi D_2 + \frac{\pi}{2} \qquad (18)$$

The fundamental is extracted in the proposed control $n = 1$:

$$A_1 = \frac{1}{\pi^2} \frac{V_{out1}}{L_2 f_{d2}} \frac{1}{(1-D_2)} \sin(\pi D_2) \qquad (19)$$

$$\varphi_1 = \pi D_2 + \frac{\pi}{2} \qquad (20)$$

After the load DC-DC converter's inductor current has been decomposed using the Fourier series, the fundamental is multiplied by a gain and subtracted from the original current. The expression for the modified ripple minimized current used in super-twist control is written as follows:

$$i_{sta} = i_{out1} - GA_1 \qquad (21)$$

Where G is a positive gain, and A_1 is the first harmonic's module.

III.2.1.5 Super Twisting Controller

The control signal u_2 of the super twisting algorithm is written as follows:

$$u_2 = u_d + u_{eq} \qquad (22)$$

Note that u_{eq} is the equivalent control proposed by Vadim Utkin in [58]. It is written as follows:

$$u_{eq} = 1 - \frac{V_{in2}}{V_{out2}} \qquad (23)$$

With $V_{in2} = V_{out1}$,

The switching control u_d is the discontinuous function given by equation (24); it is composed of a discontinuous part v_1 given in equation (25) and a continuous part v_2 given in equation (26)

$$u_d = v_1 + v_2 \qquad (24)$$

$$v_1 = -\lambda . |s|^{0.5} . sign(s) \qquad (25)$$

$$\dot{v_2} = -\gamma . sign(s) \qquad (26)$$

With s is the sliding surface given in equation (27)

$$s = i_{sta} - I_{ref2} , \text{ with } (s = I_{L2} - I_{ref2}) \qquad (27)$$

λ and γ are positive parameters; the reference current I_{ref2} is obtained using a conventional PI controller and i_{sta} is the modified inductor current.

III.2.2 Stability Proof

In this section, we prove the stability of the super twisting control system designed in the previous section. We do this by using a Lyapunov function approach.

III.2.2.1 Invariance Condition

From equation (22), the invariance condition is expressed as:

$$s = 0 \text{ and } \dot{s} = 0$$

Now, to delve deeper into the analysis, let us consider the derivative of the sliding surface, which is presented in equation (28):

$$\dot{s} = \dot{I}_{L2} - \dot{I}_{ref2} \tag{28}$$

$$\dot{s} = \dot{x}_3 - \dot{I}_{ref2} \tag{29}$$

$$\dot{s} = -\frac{(1-u_2).V_{out2}}{L_2} + \frac{V_{out1}}{L_2} - \dot{I}_{ref2} \tag{30}$$

The importance of these equations becomes evident as we explore further. We can derive:

$$\dot{s} = -\frac{(1-(u_{eq}+u_n)).V_{out2}}{L_2} + \frac{V_{out1}}{L_2} - \dot{I}_{ref2} \tag{31}$$

$$\dot{s} = \frac{V_{out2}}{L_2}u_n + \frac{V_{out1}-V_{out2}}{L_2} - \dot{I}_{ref2} + \frac{V_{out2}}{L_2}u_{eq} \tag{32}$$

III.2.2.2 Derivative of the Sliding Surface

For $\dot{s} = 0$ and $u_n = 0$, we obtain

$$u_{eq} = 1 - \frac{V_{out1}}{V_{out2}} + \dot{I}_{ref2}\frac{L_2}{V_{out2}} \tag{33}$$

$$\dot{s} = \frac{V_{out2}}{L_2}u_n \tag{34}$$

III.2.2.3 Lyapunov Function

Let us choose the Lyapunov function, such as

$$V = \frac{1}{2}s^2 \qquad\qquad (35)$$

To gauge the stability of this function, we evaluate its derivative:

$$\dot{V} = s\,\dot{s} \qquad\qquad (36)$$

One must verify the decrease of the Lyapunov function to zero. For this purpose, ensuring that its derivative is negative definite is sufficient.

$$\dot{V} = s\,\dot{s} < 0 \qquad\qquad (37)$$

$$\dot{V} = \frac{V_{out2}}{L_2}u_n s < 0 \qquad\qquad (38)$$

Replacing u_n in equation (38)

$$\dot{V} = \frac{V_{out2}}{L_2}s.(v_1 + v_2) < 0 \qquad\qquad (39)$$

$$\dot{V} = \frac{V_{out2}}{L_2}s.(-\lambda.|s|^{0.5}.sign(s) + \int -\gamma.sign(s)\,dt) < 0 \qquad (40)$$

$$\dot{V} = \frac{V_{out2}}{L_2}.(-\lambda.|s|^{0.5}|s| + \int -\gamma s.sign(s)\,dt) < 0 \qquad (41)$$

Upon careful examination, we confirm:

$$\dot{V} = -\frac{V_{out2}}{L_2}.(\lambda.|s|^{0.5}|s| + \int \gamma s.sign(s)\,dt) < 0 \qquad (42)$$

And $\dot{V}$ is a negative definite function. Therefore, the stability is well demonstrated.

III.2.3 Simulation Results
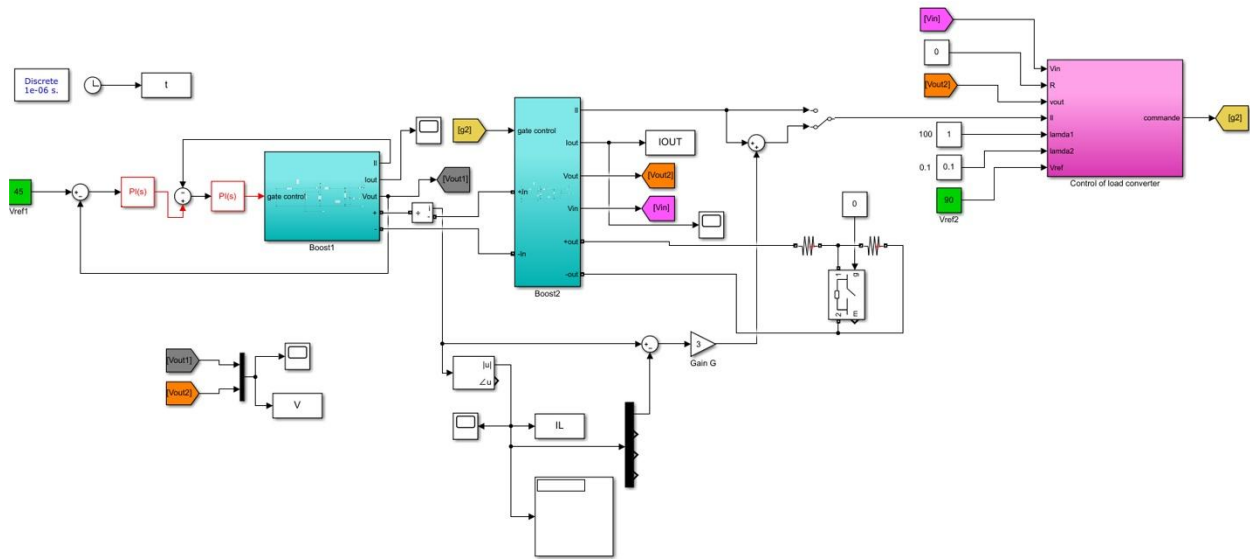
Figure III. 5. Simulation model of the proposed system

III.2.3.1 Application of the Proposed Technique for Two Different Input Voltage

Two tests were carried out without and then with the proposed new approach to ensure a fair comparison between the new technique and conventional techniques. The tests were carried out using a single harmonic injection, precisely the fundamental, and a gain of 3. The tests were carried out for two distinct values of input voltage. Initially, the 12 V input voltage was amplified to 24 V by the power supply converter. Then, the load converter amplified this 24 V voltage up to 50 V. In the second test, the power converter increased the input voltage from 24 V to 45 V. Then the load converter increased the voltage again to 90 V.

After each change of method, we examine the evolution of the outputs of the two converters: *Vout1*, *Vout2*, *IL2 (Iout1)* and *Iout2*.

III.2.3.1.1 First Level

The new Super-Twist Sliding Mode Regulator (STSMC) allows the output voltages of the supply and load converter to converge quickly and smoothly to the desired values, as shown in Figure III. 6. Figure III. 7 shows a zoom of the converter's output voltage, which behaves like a CPL. As we can see, ripple is positively impacted by the use of the new STSMC. When the suggested control strategy is applied, the ripples in the charge converter's input current (inductance current), as seen in Figure III. 8, are effectively damped. The charge converter's output current and its zoom are depicted in Figures III. 9 and 10. The ripples of this current are noticeably reduced by applying the new STSMC.
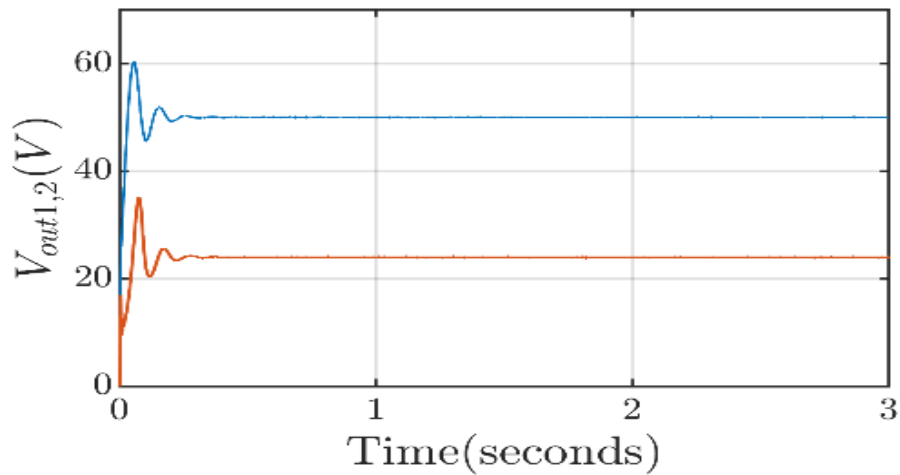
Figure III. 6. Output voltages of the supply and load converter
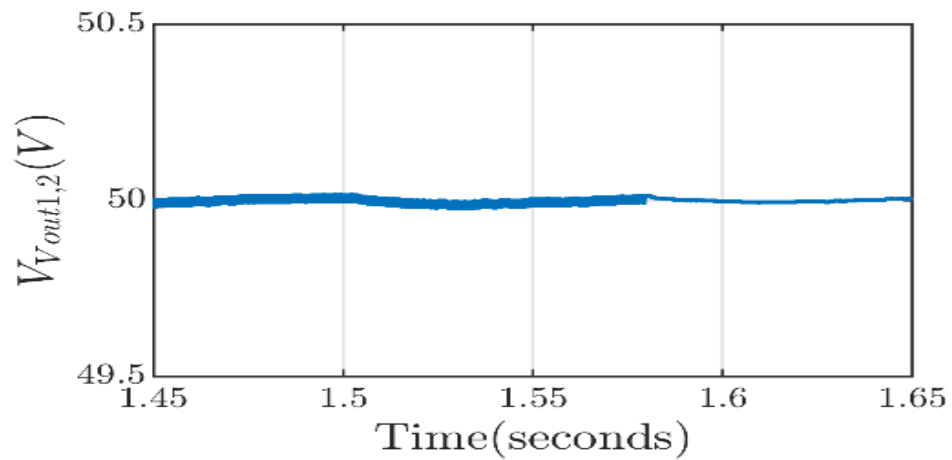
Figure III. 7. Zoom of the converter's output voltage
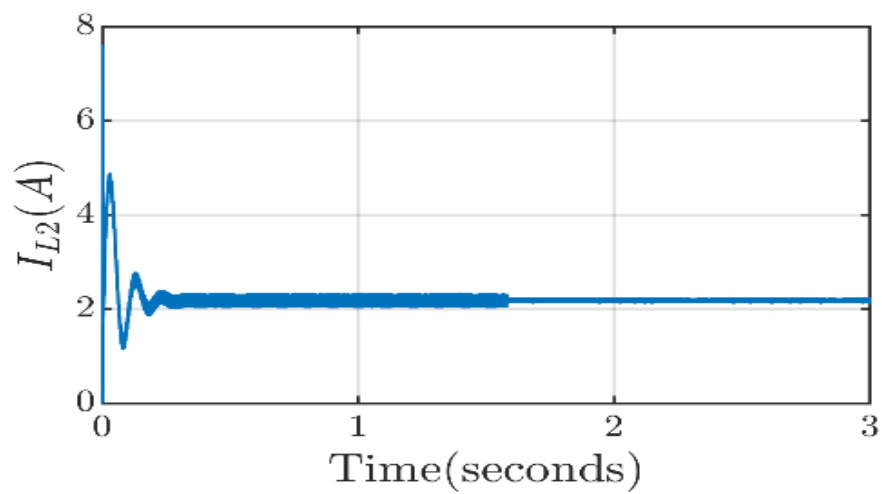
Figure III. 8. Charge converter's input current
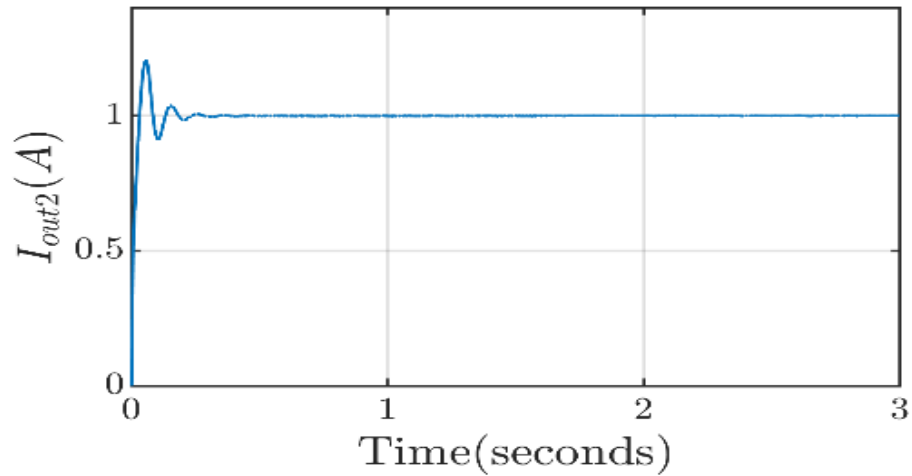
Figure III. 9. Charge converter's output current
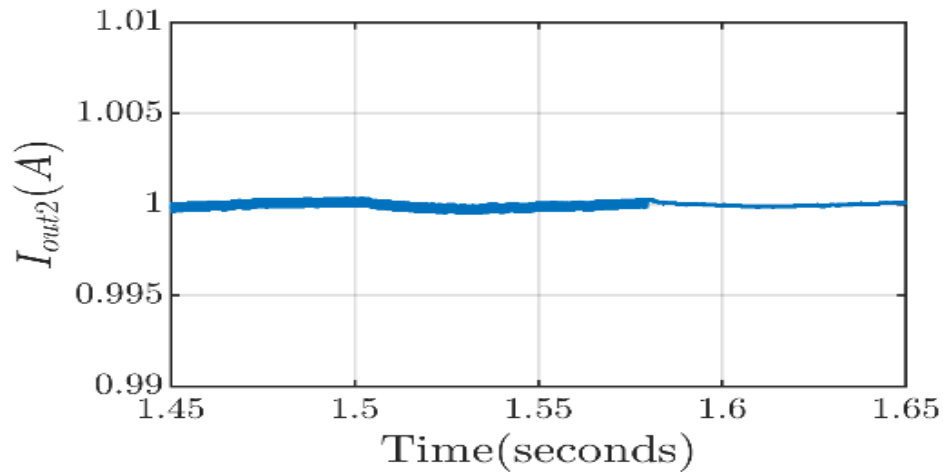
Figure III. 10. Zoom of charge converter's input current

Table III. 1 shows a comparative analysis of the amplitudes of the harmonics of the CPL input current before and after the application of the new enhancement method designed to reduce harmonics and ripples. The data shows a significant reduction in the amplitudes of each harmonic after the intervention. For example, the fundamental (1st harmonic) saw its amplitude reduced from 0.1048 to 0.02649. These results demonstrate the effectiveness of the enhancement method used, showing a substantial reduction in harmonics and ripples in the input current. This reduction in harmonics is essential for improving signal quality and the overall performance of the power system, by minimizing energy losses.

Table III. 1. Comparison of the amplitudes of the harmonics without then with the new controller

Component	Values	
	Without technique	With technique
DC	2.183	2.181
H1	0.1048	0.02649
H2	0.03805	0.009461
H3	0.02759	0.007714

III.2.3.1.2 Second Level

The previous test is repeated in this subsection, but the voltage levels are changed. The two-cascaded converters' output voltages, the CPL's input, and output currents are displayed in Figures III. 11, 12 and 13, respectively. The ripples in the input current reduced when the new STSMC was applied.
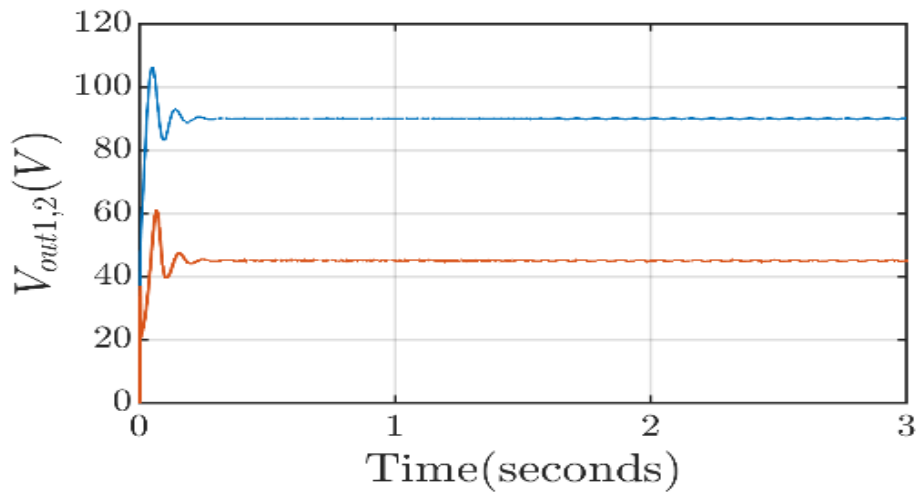
Figure III. 11. Output voltages of the supply and load converter
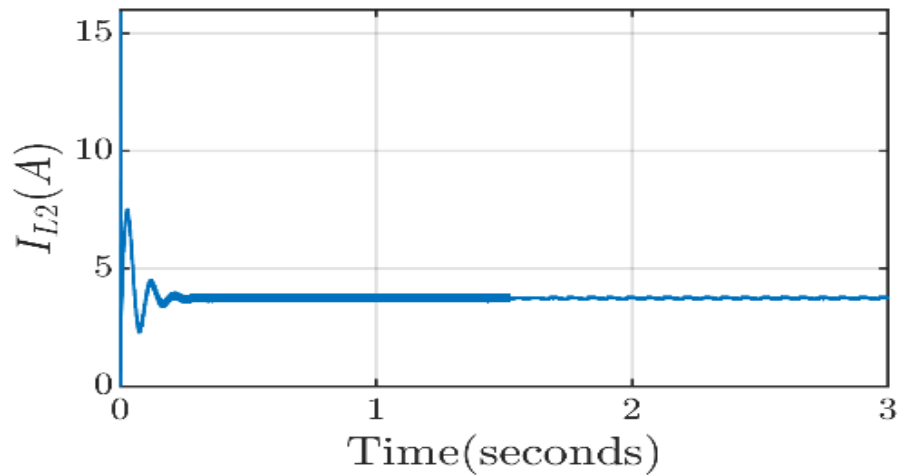
Figure III. 12. Input current of the CPL
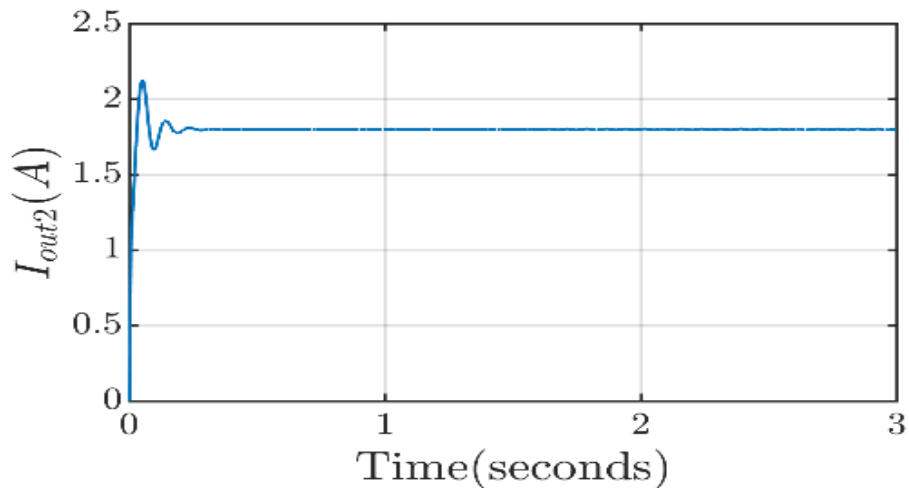
Figure III. 13. CPL's output current

A comparison of the CPL input current's harmonic amplitudes before and after the new STSMC controller was applied to reduce harmonics and ripples is displayed in Table III. 2. The data demonstrates that each harmonic's amplitude was significantly reduced following the intervention, with the second harmonic decreasing from 0.03601 to 0.01117. By minimizing energy losses, these results demonstrate the success of the enhancement method by demonstrating a significant reduction in harmonics and ripples, which is critical for enhancing signal quality and overall power system performance.

Table III. 2. Comparison of the amplitudes of the harmonics without then with the new controller

Component	Values	
	Without technique	With technique
DC	3.74	3.74
H1	0.1057	0.02892
H2	0.03601	0.01117
H3	0.0336	0.01347

III.2.3.2 Application of the Proposed Technique with Gain Variation

In the second part of the study, a simulation test was conducted to examine the effect of varying the gain G, a key element in this new control method. The results showed that with each increase in gain, the ripple of the input current to the CPL was progressively reduced. This indicates that adjusting the gain G is an effective strategy for further minimizing input current fluctuations, thereby enhancing the stability and efficiency of the power system.

The output voltages of the two converters and the input and output currents are shown in Figures III. 14, 15 and 16 respectively. The positive effect of varying the gain G is quite remarkable in the input current. As the gain increases, the ripples in the input current decrease proportionally. This relationship indicates that adjusting the gain G effectively minimizes input current fluctuations. By reducing these ripples, the stability and efficiency of the power system are significantly enhanced, leading to smoother operation and reduced energy losses.
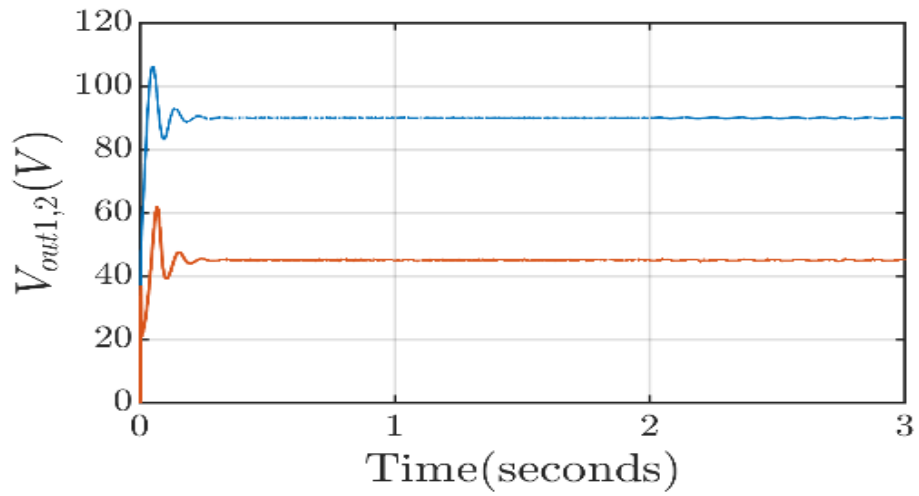
Figure III. 14. Output voltages of the supply and load converter
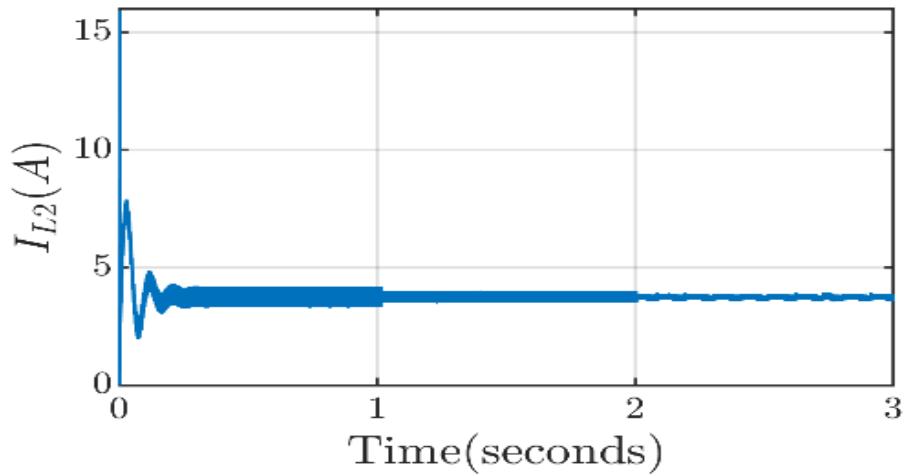
Figure III. 15. CPL's input current
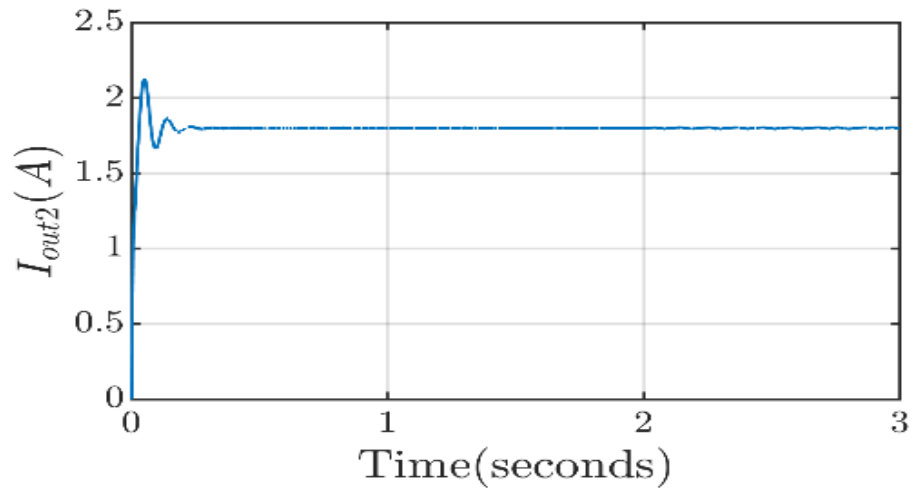
Figure III. 16. Output current of the CPL

Table III. 3 shows a comparison of the amplitudes of the harmonics for three values of gain *G*. When the gain is increased from 0.5 to 2, the amplitudes of the three harmonics are significantly reduced, each to half their initial values. The same thing happens when the gain is increased from 2 to 5. This demonstrates the effectiveness of adjusting the gain *G* in the control method. Specifically, increasing the gain proportionally reduces the amplitudes of the harmonics, thereby reducing input current ripples. This reduction is essential to improve signal quality and the overall performance of the power system. By minimizing harmonics and associated ripples, system stability and efficiency are greatly improved, resulting in smoother operation and reduced energy losses. These results highlight the importance of gain optimization in achieving optimum performance in CPL systems.

Table III. 3. Comparison of the amplitudes of the harmonics without then with the new controller

component	Values for three different gain G		
	G=0.5	*G=2*	*G=5*
DC	3.74	3.741	3.756
H1	0.3238	0.1645	0.0719
H2	0.1113	0.05747	0.02412
H3	0.08644	0.04651	0.02407

III.2.3.3 Application of the Proposed Technique under Load Variation

A robustness test is done in this sub-section, where a load change is applied to our new STSMC. The input voltage for the feeder converter is 24 V, its output is 45 V, and the output of the load converter is 90 V. The gain is fixed at 3. First, we apply the conventional STSMC. The new STSMC is then applied on a load of 73 Ω afterward, and the load is reduced to 55 Ω, leading to an increase in current. The results of the input and output voltages and currents of the load converter are shown in Figures III. 17, 18 and 19. Despite the load change, the current ripple ΔI slightly increased but remained largely under the original ripple of 5.46 A.
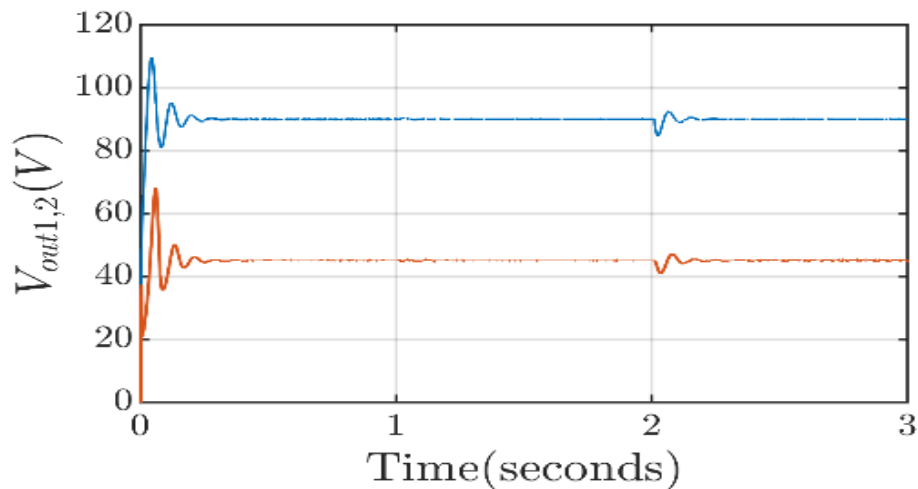
Figure III. 17. Output voltages of the supply and load converter
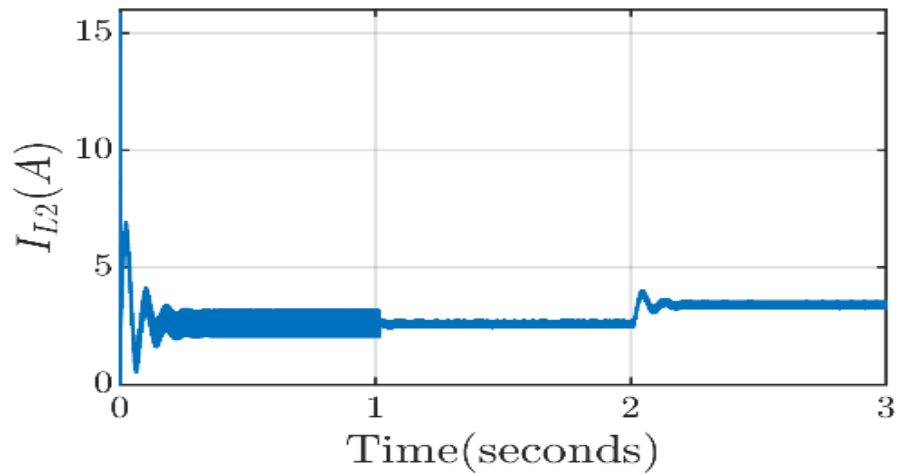
Figure III. 18. Input current of the load converter
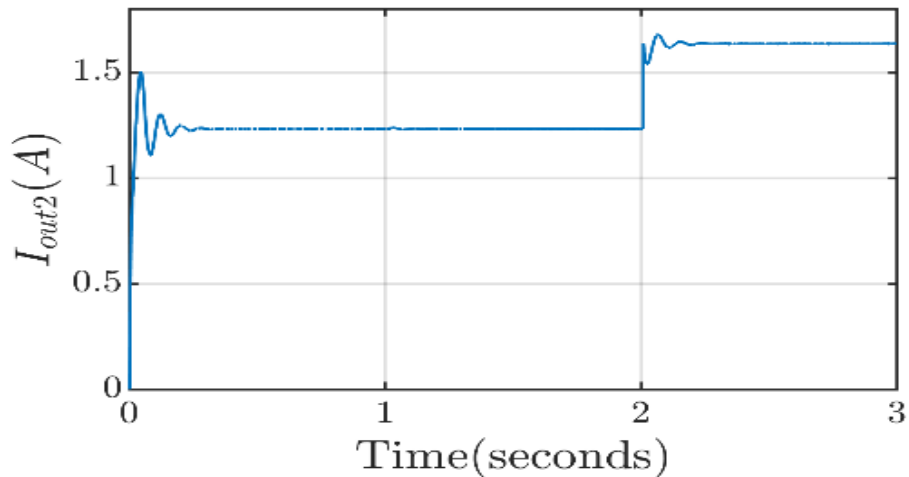
Figure III. 19. Output current of the load converter

Table III. 4 shows a comparison of the amplitudes of the harmonics without then with the new controller, for a resistance of 73 ohm, and to carry out a robustness test a resistance variation at 55 ohm is made by fixing the gain *G*. By doing this test, despite the value of the current increases, its ripple remains lower than the initial ripple (before the application of the new technique).

Table III. 4. Comparison of the amplitudes of the harmonics without then with the new controller

component	Values		
	Without technique	With technique	
	(R=73ohm)	R=73ohm	R=55ohm
DC	2.592	2.586	3.41
H1	0.478	0.1213	0.1236
H2	0.1627	0.0432	0.0487
H3	0.1101	0.0375	0.04546

III.3 Conclusion

This chapter provides a full explanation of a novel theoretical model of the present ripple minimizing method in DC microgrid. Three tests were conducted to assess the suggested technique's efficacy. In the first test, the fundamental and a gain G were injected while using the suggested method at two power levels. The second test looked at how changing the gain G multiplied by the fundamental affected the two-cascaded choppers' voltages and currents. The final test involved maintaining the input voltage and gain G constant while examining the effects of a change in the load resistance on the suggested method. We attempted to utilize a frequency of less than or equal to 10 kHz in these studies because raising the switching frequency leads to a significant loss of energy.

CHAPTER 4: Experimental Design and Results

IV.1 Introduction

The cascaded DC-DC converter, which connects several DC-DC converters via a common bus, is a key component of the distributed DC power system. The cascaded DC-DC converter's initial stage is in charge of supplying the DC bus with energy from a battery or renewable source. On the other hand, a constant power load (CPL) that uses power continuously independent of supply voltage is created when a load is connected to the DC bus in the second stage. This tendency frequently results in disruptions and instabilities, which in turn generate undesired oscillations that negatively affect the input current's quality [43]. This work suggests an active current ripple-damping method that takes the fundamental of the inductor current and uses it to solve this problem. Combined with the super-twisting sliding mode control (STSMC), this method improves the stability of the CPL and efficiently reduces ripples in the input current. This method's sliding surface selection is crucial, and it calls for the second boost converter's filtered inductor current. The efficacy of the suggested approach is illustrated by the experimental findings that are presented.

IV.2 Experiment Description

An experimental prototype shown in Figure IV. 1 is established in the LGEP laboratory to validate the proposed technique. This work uses two boost converters powered by a DC voltage source. IGBT SKM50 GB123D power switches are used. Table IV. 1 lists the nominal converter's parameters. The control algorithms are digitally implemented in a digital platform (dSPACE1104) that generates the control signals for the switches obtained by the cascaded PI and super-twisting controllers. Table IV. 2 shows the control parameters of the two cascaded converters.

Table IV. 1. Nominal converter parameters

Circuit parameters	Value
Input voltage, V_{in} (V)	12 and 24
Inductors, $L = L_1 = L_2 (mH)$	1

Internal resistance of inductances $r_L = r_{L1} = r_{L2}$ (Ω)	0.4
Capacitors, $C = C_1 = C_2 (\mu F)$	470
Load resistor, R_2 (Ω)	55, 73, and 110
The feeder chopper's switching frequency, $f_{d1}(KHz)$	10
The load chopper's switching frequency, $f_{d2}(KHz)$	5

Table IV. 2. The control parameters

Cascaded PI controller	Cascaded PI-STC
$K_{pv} = 20$	$K_{pv=}0.8$
$K_{iv} = 0.08$	$K_{iv} = 10$
$K_{pi} = 20$	$\lambda = 1$
$K_{ii} = 0.08$	$\gamma = 0$
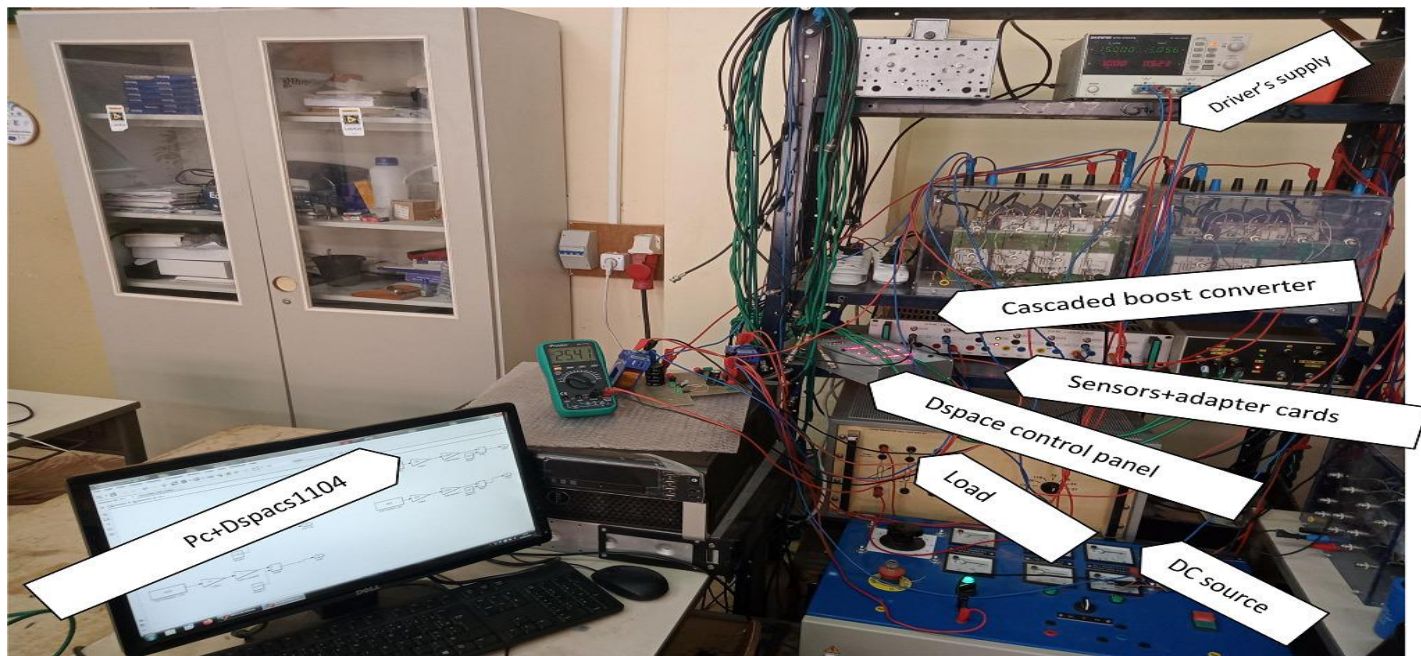
Figure IV. 1. The experiment prototype

The experimental prototype (Figure IV. 1) consists of the following items:

- ➢ dSPACE 1104.
- ➢ An autotransformer as the main grid.
- ➢ Inductors.
- ➢ Capacitors.
- ➢ Variable resistor.
- ➢ Semikron based on IGBT SKM50 GB123D.
- ➢ Driver's DC supply.
- ➢ Adapter card (Isolation card).
- ➢ Electronic card to sense the currents (LEM LA55-P) and voltages (LEM LV25-P).

IV.3 Characteristics of the Digital Controller used (DSPACE 1104)

With a 603 PowerPC floating-point processor operating at 250 MHz, the DS1104 R&D Controller Board is a standard board that can be plugged into a PCI slot. It is specifically made for the development of high-speed multivariable digital controllers and real-time simulations in a variety of fields. The board has a slave-DSP subsystem based on the TMS320F240 DSP microcontroller for advanced I/O purposes.Their advantages include [66]:

- ➢ Great flexibility of use in control development,
- ➢ Implementation of control laws after having read the algorithm in matlab/Simulink,

In our case, the control part of the entire test system is based on the Dspace 1104 control board integrated into the PC. The Dspace 1104 board contains:

Eight 16-bit analogue-to-digital converters (ADCs),

Eight 16-bit digital-to-analogue converters (DACs),

A Motorola PowerPC 603e microprocessor (250 MHz) and a Texas Instruments TMS 320F240 DSP (20 MHz), which handles the digital I/O,

- ➢ Two 16-bit I/O ports collect information from the incremental encoder,
- ➢ Two RS 232 and RS 485 serial ports,

➢ One slave port used to generate PWM signals.

The computer acts as a Human/Machine interface and controls the entire control process. Its main functions can be summarized as follows:

➢ Programming of control law algorithms using Matlab/Simulink,

➢ Compilation, code generation and linking with the Texas Instruments compiler dedicated to TMS320 processors,

➢ Loading the application into the memory of the Dspace 1104 control board and its control, Data acquisition and sketching of the various signals using ControlDesk

The isolation card between the dSPACE 1104 and the inverter ensures overvoltage protection, ground separation and system safety by electrically isolating the two components.

IV.4 Experimental Results and Discussion

Three experiments were conducted to assess the efficiency of the proposed technique, using the experimental setup illustrated in Figure IV. 2. These tests were designed to investigate the performance of the system under different conditions by varying key parameters. The first test involved applying the method suggested in the previous chapter to two power levels by injecting the fundamental and a gain G equal to 2. The second test examined the effect of a variation of the gain G multiplied by the fundamental on the voltages and currents of the two cascaded choppers. The last test involved checking the impact of a load resistance variation on the proposed technique while keeping the gain G and input voltage fixed. In these tests, we used a frequency less than or equal to 10 kHz, because the elevation of the switching frequency induces a significant loss of energy.
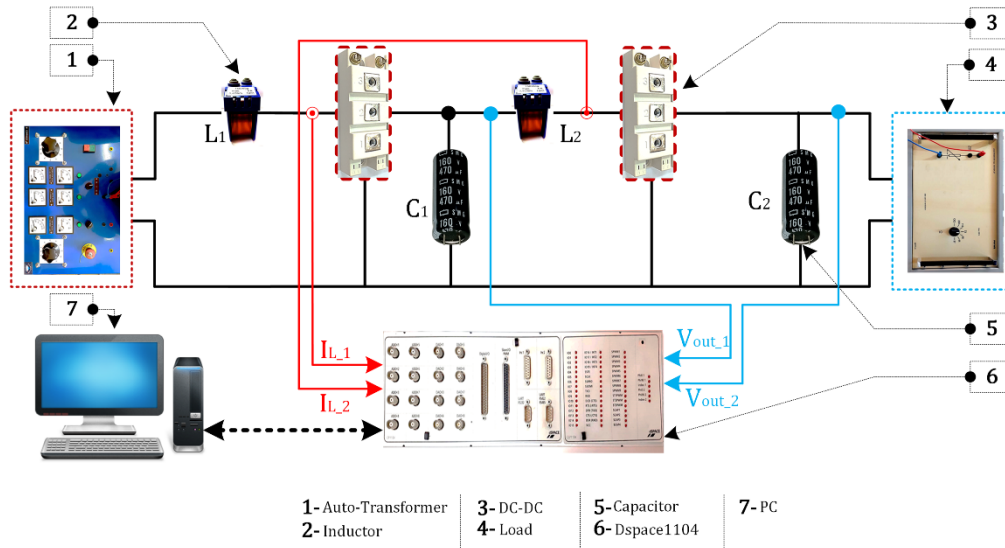
Figure IV. 2. Schematic of the experimental setup

IV.4.1 Application of the Proposed Technique for Two Different Input Voltage

A test was conducted with and without the proposed approach to ensure a fair comparison between the novel and conventional techniques. The test was achieved using a single harmonic injection, precisely the fundamental, and a gain of 2. The test was performed at two distinct input voltage values. Initially, the input voltage of 12V was amplified to 24V by the feeder converter. Subsequently, the load converter further boosted this 24V to 50V. Secondly, the feeder converter increased the input voltage from 24V to 45V. Later, the load converter further elevated the voltage to 90V.

After each method switch, we examine the evolution of the outputs of the two converters: *Vout1, Vout2, IL2 (Iout1),* and *Iout2.*

Figure IV. 3 shows the outputs of the first converter (feeder converter). Using a gain of 2, the new STSMC affected the first converter and reduced the output voltage by 60% and the output current by 73% in the case of *V$_{in1}$=12V*. For *V$_{in1}$=24V, V$_{out1}$* ripples were decreased by 57%, and *Iout$_1$* ripples by 84%. (The ripples *ΔV* and *ΔI* are reduced from 10V to 4V and from 5.46A to 1.5A in the case of *V$_{in1}$=12V*. In the case of V$_{in1}$=24V, the ripples *ΔV* and *ΔI* are reduced from 14V to 6V and 10A to 1.65A).
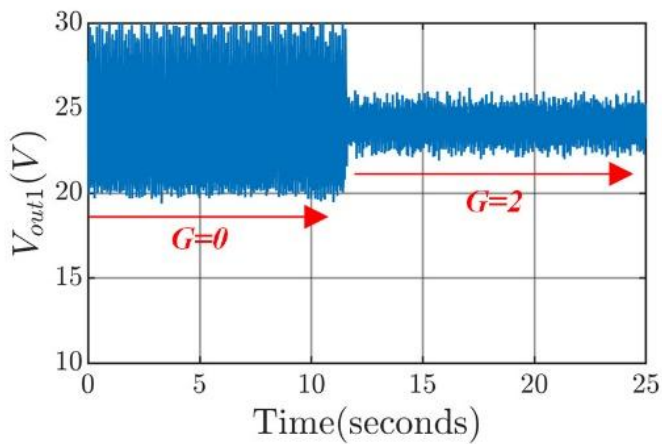
(a)
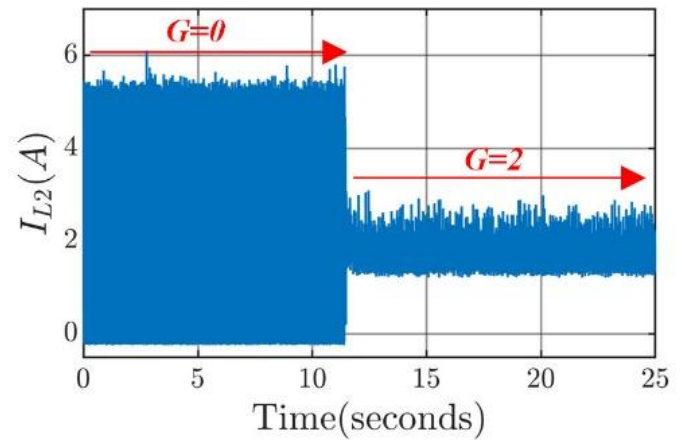
(b)
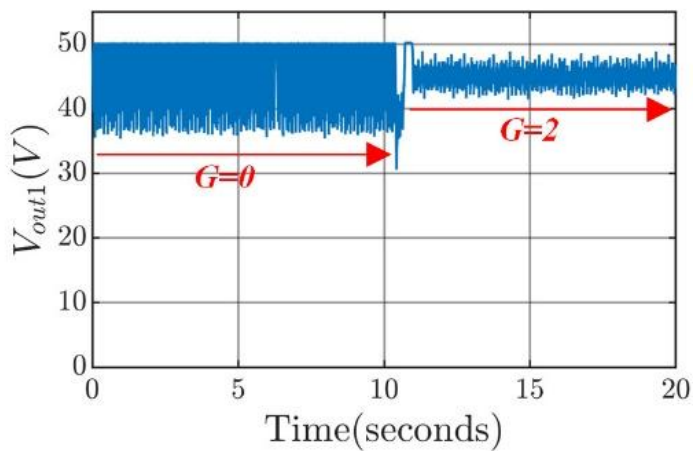
(c)
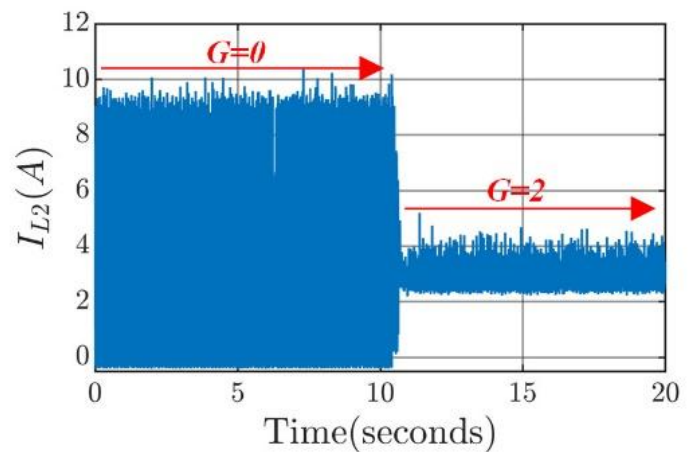
(d)

Figure IV. 3. Outputs of the feeder converter using the conventional STSMC then the new STSMC: $V_{in1}=12V$ input: (a): The output voltage, (b): the output current. $V_{in1}=24V$: (c): The output voltage, (d): the output current

Figure IV. 4 shows the outputs of the load converter. The new STSMC reduced this converter's output voltage and current by 48% (ΔV is reduced from 6.08V to 3.36V) and by 56% (ΔI is reduced from 0.09A to 0.05A) in the case of $V_{in1}=12V$. In the case of $V_{in1}=24V$, the output voltage and current are reduced by 60% (ΔV is reduced from 10.71V to 3.83V) and by 68 % (ΔI is reduced from 0.17A to 0.06A). For both input voltage levels, the new active control method based on a suitable choice of sliding surface used in super twisting control and fundamental extraction has effectively reduced current and voltage ripples.
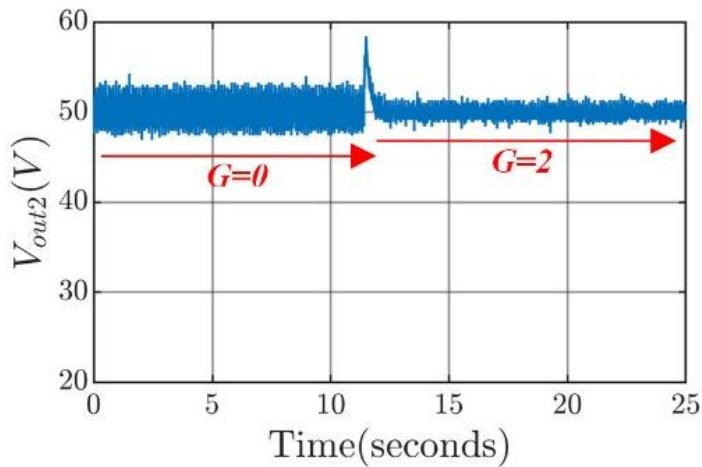
(a)
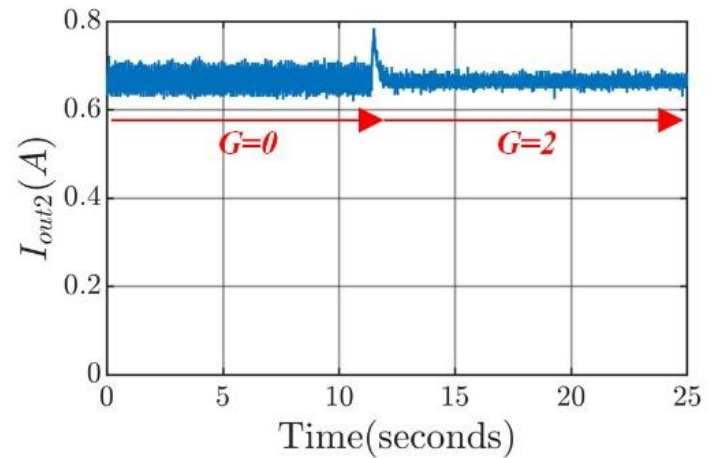
(b)
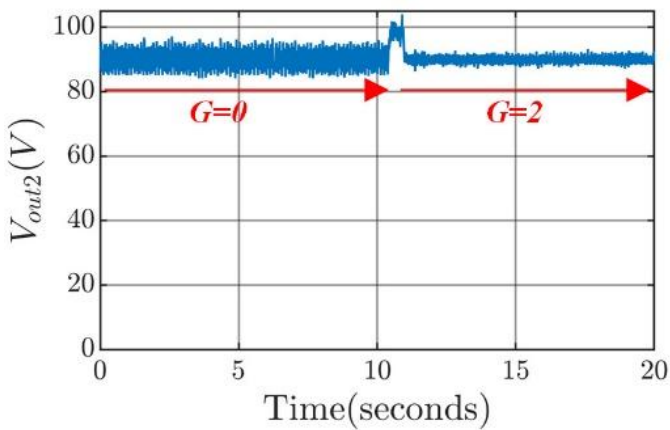
(c)
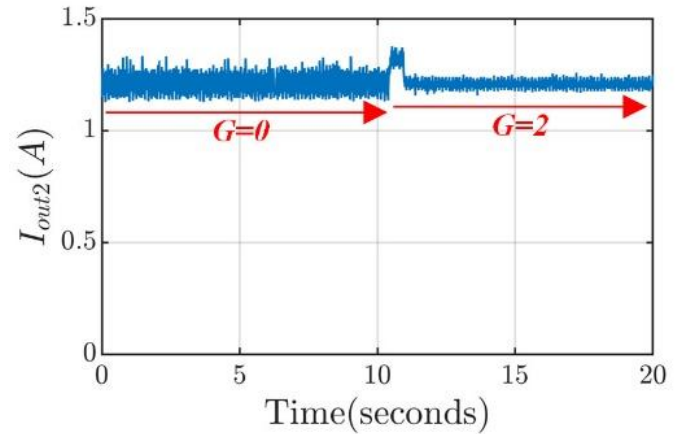
(d)

Figure IV. 4. Outputs of the load converter using the conventional STSMC then the new STSMC: $V_{in1}=12V$ input: (a): The output voltage, (b): the output current. $V_{in1}=24V$: (c): The output voltage, (d): the output current

IV.4.2 Effect of the Gain Variation on the Voltages and Currents of the Two Converters

After confirming the effectiveness of the new STSMC in reducing the ripples of the different voltages and currents in our system, it is time to check the effect of the gain G.

Rising the gain from 1 to 2 had a noticeable effect on the input current of the load converter. The ripple ΔI is reduced by 56% (from 3.38A to 1.5A).

Other outputs were slightly affected, as shown in Figure IV. 5.

76

Increasing the gain to 3 did not affect the outputs of the two converters.
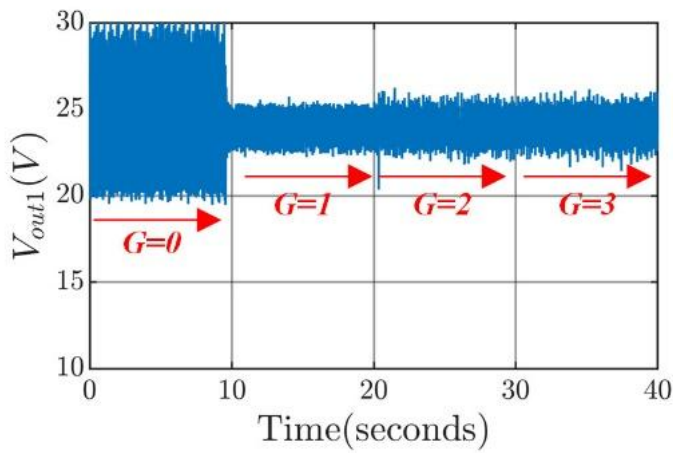
(a)
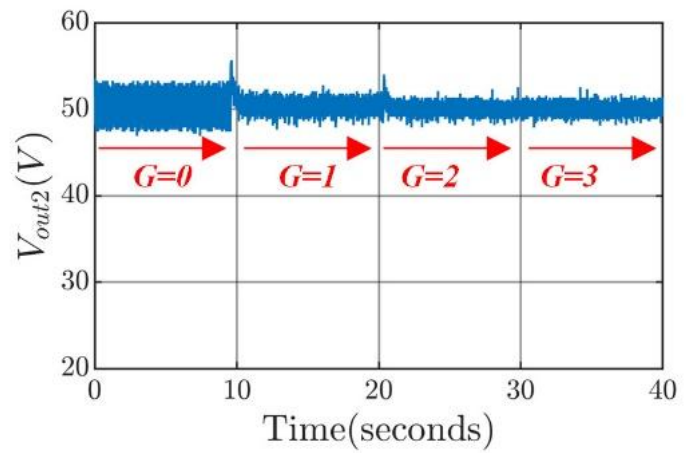
(b)
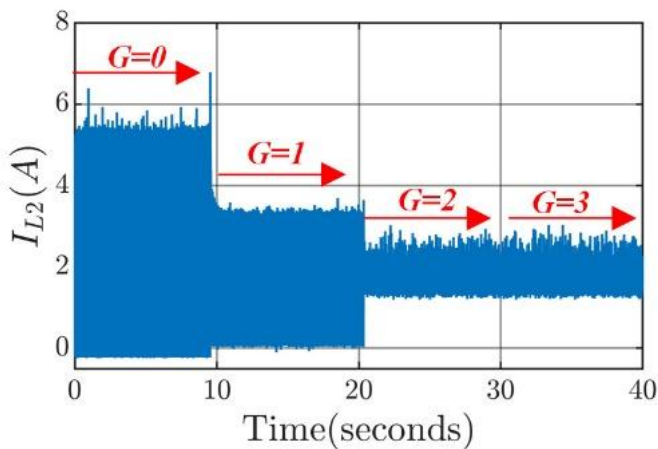
(c)
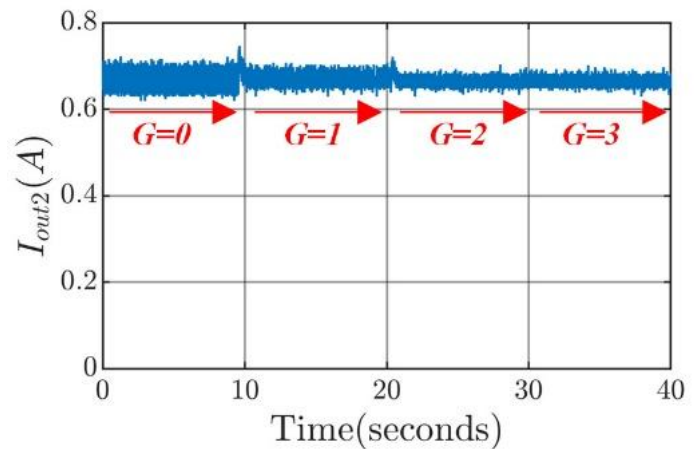
(d)

Figure IV. 5. The effect of increasing the gain *G* (values 1, 2 and 3): (a): The feeder converter's output voltage, (b): the load converter's output voltage, (c): The load converter's input current, (d): The load converter's output current

IV.4.3 Control of the Converters under Load Variation

A robustness test is done in this part, where a load change is applied to our new STSMC. The input voltage for the feeder converter is 12V, its output is 24V, and the output of the load converter is 50V. The gain is fixed at 2.

First, we apply the conventional STSMC, the new STSMC is applied on a load of 73 Ω afterward, and the load is reduced to 55 Ω leading to an increase of the current. The results of the input and

output voltages and currents of the load converter are shown in Figure IV. 6. Despite the load change, the current ripple ΔI slightly increased (1.5A to 1.62A) but remained largely under the original ripple of 5.46A.
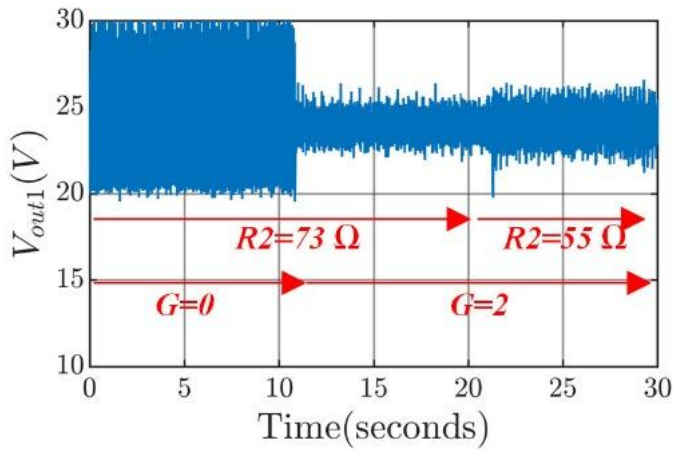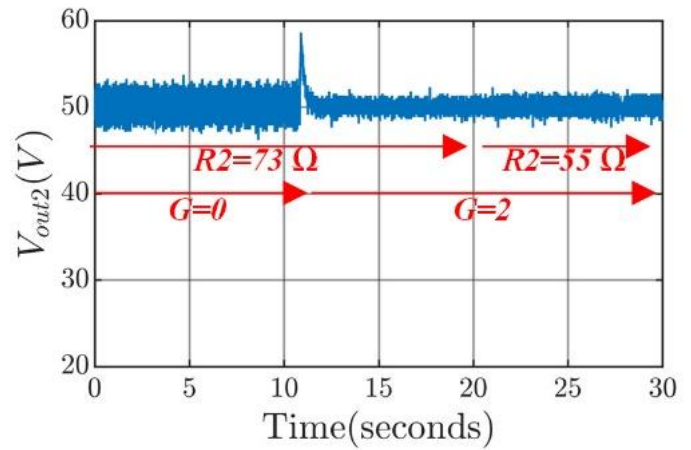
(a)   (b)
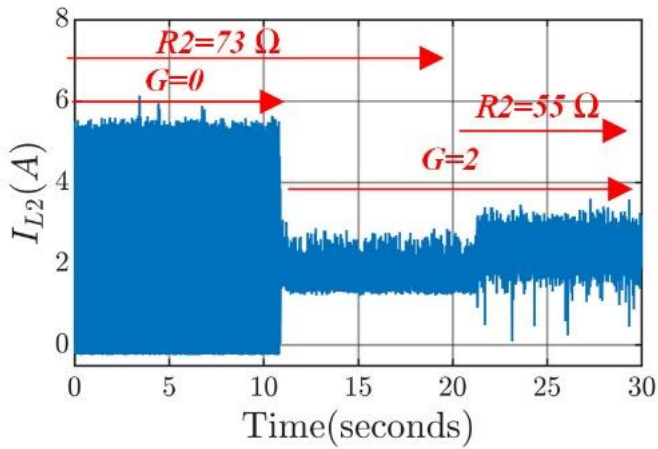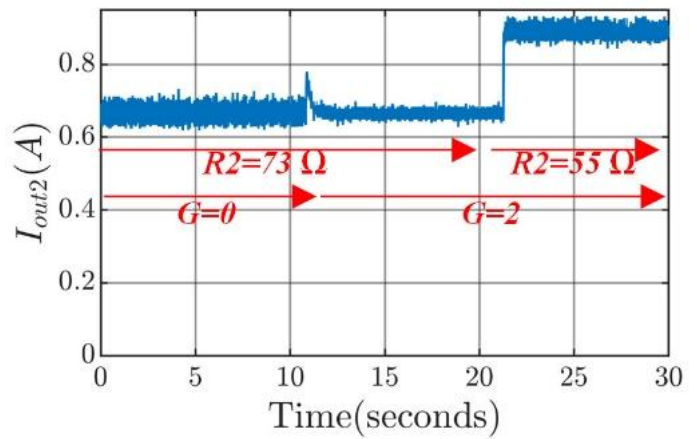
(c)   (d)

Figure IV. 6. Load change test with a gain $G=2$: (a): The feeder converter's output voltage, (b): the load converter's output voltage, (c): The load converter's input current, (d): The load converter's output current.

IV.5 Discussion

Experimental tests shown above gave insight into the merits of the new STSMC. Our main goal was to reduce the input current of the load converter (I_{L2} or I_{out1}). However, lowering the input voltage V_{out1} and hence the output current and voltage (I_{out2} and V_{out2}) was a by-product of this operation.

78

Figure IV. 7 resume visually the experimental tests. To represent the amount of ripple reduction, a new quantity has been bar plotted; this quantity is defined as:

$$\text{Amount of ripple reduction} = \frac{\Delta X_{STSMC} - \Delta X_{new-STSMC}}{\Delta X_{STSMC}} \quad (43)$$

(a)

(b)
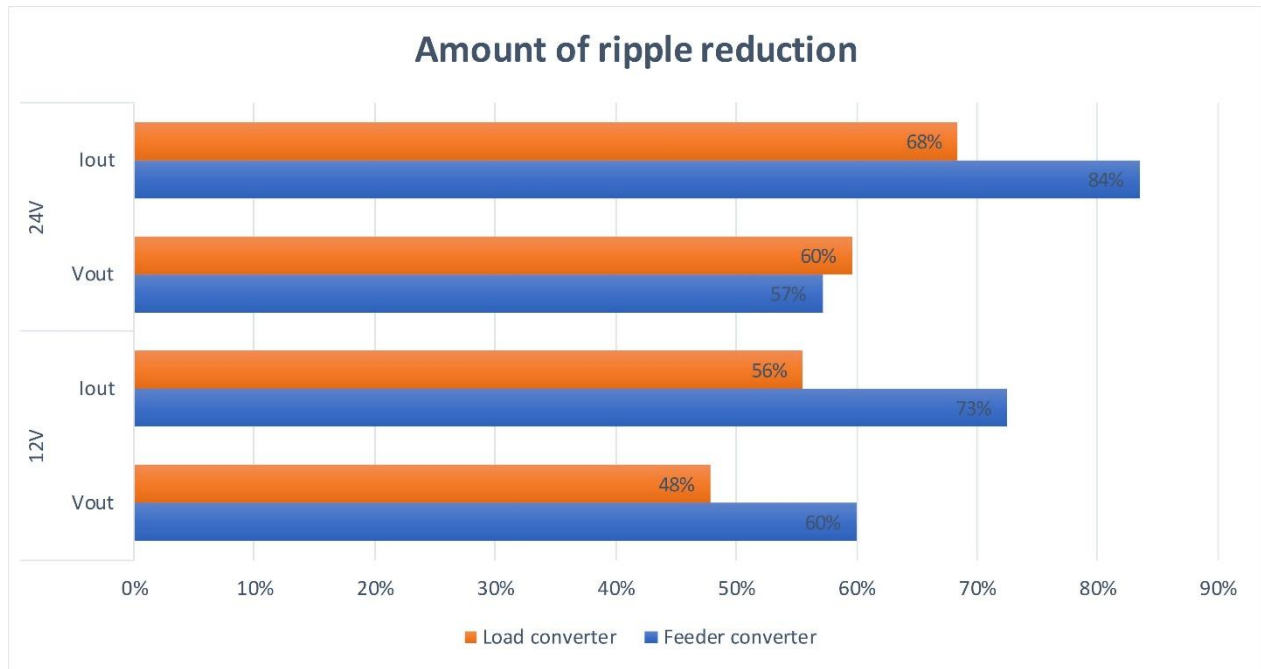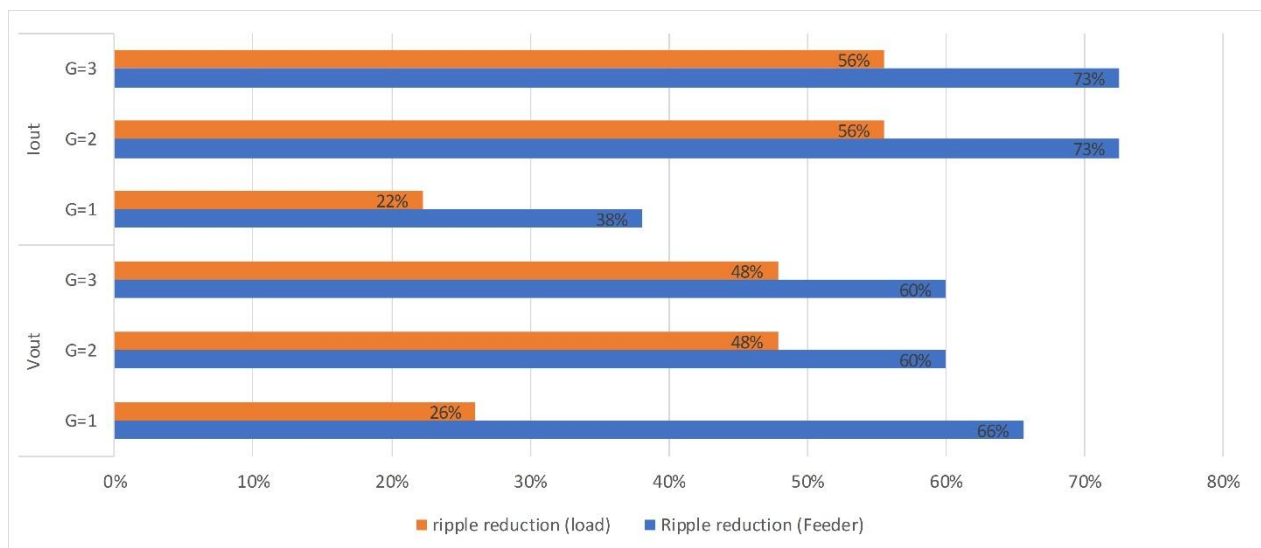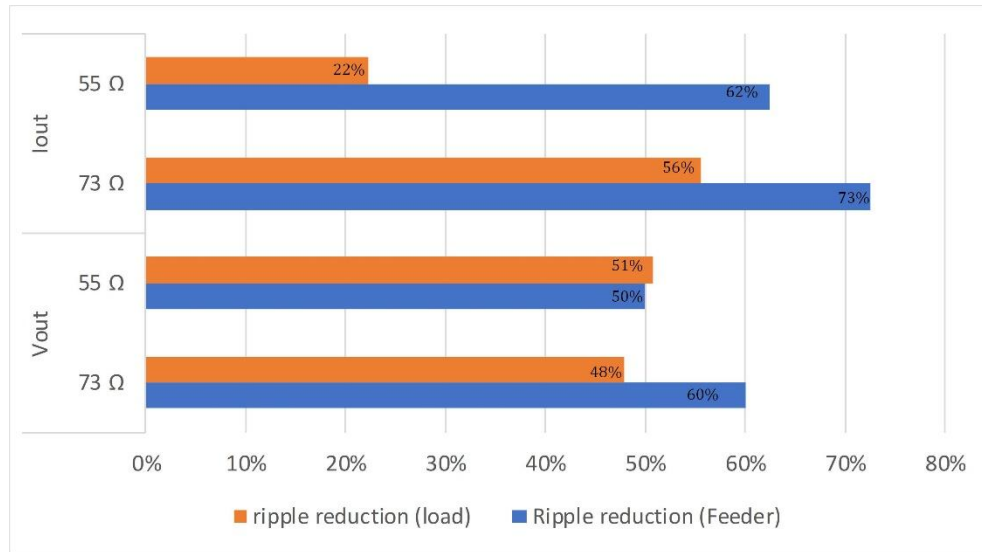
(c)

Figure IV. 7. Ripple reduction in the case of: (a) Voltage change. (b) Gain change. (c) Load change

Analysing the experimental results yield the following conclusions:

➢ The modified super twisting is robust to input and output voltage changes. During the experimental tests, the controller maintained consistent performance when the input voltage of the load converter increased from 24V to 45V, with a corresponding rise in output voltage from 50V to 90V. This ability to adapt to a wide range of operational voltages without significant degradation in performance or stability is a practical demonstration of its robustness.

➢ The input voltage of the load converter has been increased from 24V to 45V resulting in a change of the output voltage from 50V to 90V. Even though there was a surge in ΔI, the proposed modified super twisting kept a high current ripple reduction. While an increase in input voltage may lead to a surge in current ripple (ΔI) due to higher energy transfer, the sliding surface and gain adjustments in the modified super-twisting method effectively suppress the ripple. This performance demonstrates the controller's capacity to mitigate disturbances even under higher voltage conditions.

➢ As mentioned at the beginning of the section, reducing the input current affected the other currents and voltages, resulting in a positive ripple reduction in these outputs.

➢ A gain of 2 is the optimal gain. We noticed a surge in ripple reduction when we increased the gain from 1 to 2. Further increases had no effect.

➢ The modified super twisting moved the load converter's inductor current away from 0, making it a suitable method to avoid discontinuous conducting mode. During the practical implementation, it was observed that the inductor current remained above zero even under varying input and load conditions. This empirical evidence reinforces the effectiveness of the proposed control strategy in maintaining system stability and avoiding DCM.

IV.6 Comparison Assessment with Other Solutions

Table IV. 3. Comparison of the proposed controller's parameters with various controllers used in the high gain boost converter

References	Topology	Active/Passive damping or new converter topology	Control	Voltage gain	Amount of ripple reduction	L/C	S/D	Total	Efficiency (%)
[67]	Two stage cascaded boost converter	Active	A classic controller PI	4	Inductor current not measured	2/2	2/2	8	Not mentioned
[68]	Two stage cascaded boost converter	Active	Flatness-Based Decentralized Adaptive Backstepping Controller	2	++ for DABC+LPs (Vref variation). + for DABC+LPs (Load variation). ++ for DABC+LPs (E variation).	2/2	2/2	8	Not mentioned

					+ for SMBC (Vref variation).				
[69]	Two stage cascaded boost converter	Active	A feedback controller composed of a comparator and an RS flip-flop	3.5	+++ for SF. ++ for DF.	2/2	2/2	8	Not mentioned
[70]	Two stage cascaded boost converter	Active	A PI and sliding mode controllers	2	+++	2/2	2/2	8	Not mentioned
[71]	Two parallel boost converters	Passive	A passive feedforward controller is added to the conventional double loop controller	2	+++	2/2	2/2	8	Not mentioned
[72]	A new dual-input high step-up DC–DC converter	New converter topology	A classic controller PI	14.64	+++	2/5	2/4	13	96.35
[73]	An ultra-high gain dc/dc boost converter with a modified voltage multiplier cell (VMC)	Active	A classic controller PI	9.75	+++	2/6	1/7	16	95.4

[74]	CI-SIDO boost converter	Active	The controller is implemented in FPGA mainly using registers, discrete counters and comparators.	2.25	+++	2/2	2/2	8	87.5
[75]	A new single-switch non-isolated DC/DC converter	New converter topology	A conventional PWM technique at a constant frequency	10	+++	2/4	1/3	10	95.8
Proposed [76]	Two stage cascaded boost converter	Active	A PI and a new super twisting controllers.	4	++ for G=1. +++ for G=2. +++ for G=3.	2/2	2/2	8	90.28

To calculate overall circuit efficiency, we need to calculate the power output by the second boost converter and the power absorbed by the first converter, and then we divide it up.

The power output by the second boost converter is equal to 50V*0.65A=32.5watt. The power absorbed by the first boost converter is equal to 12V*3A=36watt. So the efficiency is equal to 90.28% (mentioned in the table).

Efficiency without using technique is about 88.09%, after using the proposed technique it came 90.28%. For the prototype used in this paper, the proposed technique increased the efficiency by 2%.

Efficiency can never reach 100% because in every converter, there are components that reduce efficiency, such as semiconductors (2 diodes and 2 IGBTs in our case). Energy conversion electronics are based on the use of semiconductor components acting as switches. When these switches are in use, they suffer thermal losses corresponding to the various phases of their operation. There are three types of loss, each corresponding to a different state of the switch:

Conduction losses, associated with the conducting state of the component.

Leakage losses, associated with the blocked state of the switch.

Dynamic losses, or switching losses, associated with changes in the state of the switch, i.e. when passing from the on state to the off state and vice versa.

These losses cause a considerable reduction in the system's overall performance.

It is interesting to compare some of the solutions done in the past with the work we have done to enhance the value of paper. Table IV. 3 summarizes the performances of the ripple minimization technique mentioned in the literature, control method, efficiency measurement and voltage gain ratio. Metrics are displayed in Table 3 are taken from data provided by authors in their papers.

In [67, 68, 69, 70] and the present paper, the use of two classic boost converters operating in cascade increased the voltage gain between 2 and 4, using the same number of diodes, switches, inductors, and capacitors. Since the inductor current in [67] is not measured, its ripple could not be determined. In [68], for a variation of input or output voltage, the DABC+LPs allow a slight reduction of the current ripple, while the SMBC does not give a good reduction. In [69], the current ripples are reduced for different frequencies and are well reduced for the same frequencies, but the control method is a bit more complex. The observed reduction in current ripples across varying and consistent frequencies can be attributed to the efficiency of the control algorithm in adapting to frequency changes, effectively minimizing disturbances. Although the current ripples are well reduced in [70], using high frequencies (100 KHz) can increase the energy losses, reducing the system's efficiency. The control of the two converters connected in parallel in [71] consists in adding a passive controller to the conventional double-loop regulator. This type of control allows a very minimal current ripple, guaranteeing a positive reality in the system transfer function, simplifying control design and improving controllability. But its problem is the power dissipation. The use of a new topology, a new dual-input high-amplification-rate DC-DC converter controlled by a conventional pi regulator with an efficiency of 96.35% [72], and an ultra-high-gain DC/DC boost converter with a modified voltage-multiplying cell (VMC) with an efficiency of 95.4% [73], provide high voltage gain with reduced current ripple. However, the drawback of these two works is the use of a large number of components. The CI-SIDO converter presented in [74] allows a voltage gain of 2.25 with a reduced number of components (8) and a low current ripple with an

efficiency of 87.5%. The ripples are well reduced by adjusting the timing of the gate pulses. The new non-isolated single-switch DC/DC converter used in [75] allows for a high voltage gain with low current ripple while using 10 components with an efficiency of 95.8%. The topology features coupled inductors that significantly reduce input current ripple to near zero, while improving power density and system durability, particularly for fuel cell applications. In this work, the two-stage cascaded boost converter structure is employed with several forms of control. In this case, the voltage gain is equal to 4 with an efficiency of 90.28%, and the current ripple is well reduced after using the new inductor current ripple minimization technique. Compared to the state-of-the-art ripple minimization techniques, our method employs the converter's measured variable without the need for additional hardware or complex mathematical procedures. Moreover, it is robust to input and output voltage changes. In addition, the quality improvement effect of the current and/or voltage comes from both the load converter side and the power converter side.

IV.7 Conclusion

This chapter presents a new method for reducing ripples in a cascaded DC/DC converter. The focus is reducing the second stage's input ripple in a cascaded DC/DC boost. To achieve this, a modified super-twisting sliding mode controller (STSMC) is used, which feeds back a weighted fundamental component of the second-stage input current to reduce the input current. This reduces ripples in both the input and output voltage and current of the second stage. The novelty of this technique is the choice of the sliding surface. The technique is part of active damping approaches, does not require additional sensors or passive components, and reduces system cost. The method improves the load and power converter sides' current and/or voltage quality. It is easy to implement and is applicable to various loads and power levels. Additionally, it provides a voltage gain of 4 for frequencies of 10 kHz or less and is robust to input and output voltage changes. Experimental tests have confirmed its effectiveness, with a gain of 2 being the optimal result.

Conclusion

Conclusion

Improving the power quality of dc-dc converters is the focus of this thesis. The study in this thesis is based on the concept of a DC microgrid, based on a cascade of two dc-dc converters.

In the first chapter, we gave an overview of the DC microgrid (its different definitions, its advantages and disadvantages, its main components and its operating modes). Next, a classification of DC-DC converters is discussed, highlighting the advantages and disadvantages of each type in terms of performance and ripple current. In the third part of this chapter, power quality issues in dc systems were discussed, and various dc-dc converter control strategies were presented. This chapter was concluded with a critical review of the various existing techniques for the minimization of current ripple in dc-dc converters by assessing their performance, complexity and applicability to dc microgrids.

In the second chapter, a basic DC microgrid structure is studied, three control methods have been realized under the variation of the input voltage of the overall system in order to compensate the destabilizing effect of constant power loads. The simulation results of the cascade PI controller showed that this type of control guarantees good accuracy with high efficiency. For the system controlled by the sliding mode, severe unstable fluctuations in voltage and current occurred, but the system speed was improved compared with the first controller. The super torsion controller guarantees good accuracy and stability with a lower ripple factor of the load converter inductance current (LCC), the disadvantage of this control is that it is a little slow compared with the other two types of control.

A theoretical model of the DC microgrid current ripple minimisation technique is detailed in the third chapter. To evaluate the effectiveness of the proposed technique, three tests were carried out. The first test involved applying the proposed method at two power levels by injecting the fundamental and a gain. The second test examined the effect of varying the gain G multiplied by the fundamental on the voltages and currents of the two cascaded choppers. The final test involved checking the impact of varying the load resistance on the proposed technique while keeping the gain and input voltage fixed.

In the final chapter, an experimental prototype is set up in the LGEP laboratory to validate the technique proposed in chapter three. The novelty of this technique lies in the choice of the sliding surface. The technique is one of the active damping approaches, does not require additional sensors or passive components and reduces the cost of the system. Experimental results confirm that the proposed new method improves current and/or voltage quality on both the load and power converter sides. It is easy to implement and can be applied to different loads and power levels. In addition, it provides a voltage gain of 4 for frequencies of 10 kHz or less and is robust to changes in input and output voltage. Experimental tests have confirmed its effectiveness, with a gain of 2 being the optimum result.

There are still a number of research avenues that can be explored in the context of this work. Here are a few suggestions:

Improve the experimental bench by integrating renewable energy sources

Use super capacitors instead of the capacitors used in this work

Use another type of battery by integrating advanced controls based on artificial intelligence for the control of interleaved converters.

Bibliography

[1] Al-Ismail, F. S. (2021). DC microgrid planning, operation, and control: A comprehensive review. *IEEE Access*, *9*, 36154-36172.

[2] Whaite, S., Grainger, B., & Kwasinski, A. (2015). Power quality in DC power distribution systems and microgrids. *Energies*, *8*(5), 4378-4399.

[3] AL-Nussairi, M. K., Bayindir, R., Padmanaban, S., Mihet-Popa, L., & Siano, P. (2017). Constant power loads (cpl) with microgrids: Problem definition, stability analysis and compensation techniques. Energies, 10(10), 1656.

[4] Siad, S. B. (2019). DC MicroGrids Control for renewable energy integration (Doctoral dissertation, Université Paris-Saclay; Université d'Evry.

[5] JL. Soon, GP. Raman, JCH. Peng, and DDC. Lu, "Current Ripple Reduction Using AC Core Biasing in DC–DC Converters" IEEE Trans. Ind. Electron, vol. 68, no. 10, 10058 10067,2020.

[6] X. Cao, Q. Zhong, W. Ming, "Ripple eliminator to smooth DC-Bus voltage and reduce the total capacitance required", IEEE Trans. Power Electron, vol. 62, no. 4, 2224-2235, 2015.

[7] A.Vicenzutti, D. Bosich, AA. Tavagnutti, and G. Sulligoi, "System Stability and Short Circuit Contribution as Discordant Targets in Cascade Connected DC Microgrids: a Design Procedure". In 2022 International Conference on Smart Energy Systems and Technologies (SEST), 1-6, 2022

[8] L. An, and DD. Lu, "Analysis of DC Bus Capacitor Current Ripple Reduction in Basic DC/DC Cascaded Two-Stage Power Converters" IEEE Trans. Ind. Electron, vol. 63, no. 12, 7467-7477, 2016.

[9] Siad, S. B. (2019). DC MicroGrids Control for renewable energy integration (Doctoral dissertation, Université Paris-Saclay; Université d'Evry).

[10] Ertekin, D. (2023). A high gain switched-inductor-capacitor DC-DC boost converter for photovoltaic-based micro-grid applications. CSEE Journal of Power and Energy Systems.

Bibliography

[11] Nath, S. (2021). Maximizing ripple cancellation in input current for SIDO boost converter by design of coupled inductors. IEEE Journal of Emerging and Selected Topics in Industrial Electronics, 2(4), 409-419.

[12] Braitor, A. C. (2022). Advanced hierarchical control and stability analysis of DC microgrids. Springer Nature.

[13] Asmus, P. (2010). Microgrids, virtual power plants and our distributed energy future. The Electricity Journal, 23(10), 72-82.

[14] Sahoo, S. K., Sinha, A. K., & Kishore, N. K. (2017). Control techniques in AC, DC, and hybrid AC–DC microgrid: A review. IEEE Journal of Emerging and Selected Topics in Power Electronics, 6(2), 738-759.

[15] Bolboceanu, D. B. (2017). Voltag Droop Control Design for DC Microgrids (Master's thesis, Universitat Politècnica de Catalunya).

[16] Ali, S., Zheng, Z., Aillerie, M., Sawicki, J. P., Pera, M. C., & Hissel, D. (2021). A review of DC Microgrid energy management systems dedicated to residential applications. Energies, 14(14), 4308.

[17] Vijayaragavan, K. P. (2017). Feasibility of DC microgrids for rural electrification.

[18] Mohammadi, J. (2019). Integrity Protection of the DC Microgrid (Doctoral dissertation, The University of Western Ontario (Canada)).

[19] Otten, V. (2020). Power sharing in DC microgrids (Doctoral dissertation).

[20] H. Nikkhajoei, and R. H. Lasseter, "Distributed generation interface to the CERTS microgrid," IEEE Trans. Power Del., vol. 24, no. 3, pp. 1598–1608, 2009.

[21] ALSHIREEDAH, A. M. (2021). IMPROVE CONTROL STRATEGY FOR POWER SHARING IN ISLANDED MICROGRID (Doctoral dissertation).

[22] Bahij, Z. (2021). DC Microgrid Modeling and Control in Islanded Mode. Rochester Institute of Technology.

Bibliography

[23] Rajesh, K. S., Dash, S. S., Rajagopal, R., & Sridhar, R. (2017). A review on control of ac microgrid. Renewable and sustainable energy reviews, 71, 814-819.

[24] Parvez, M., Pereira, A. T., Ertugrul, N., Weste, N. H., Abbott, D., & Al-Sarawi, S. F. (2021). Wide bandgap DC–DC converter topologies for power applications. Proceedings of the IEEE, 109(7), 1253-1275.

[25] Paez, J. D., Frey, D., Maneiro, J., Bacha, S., & Dworakowski, P. (2018). Overview of DC–DC converters dedicated to HVdc grids. IEEE Transactions on Power Delivery, 34(1), 119-128.

[26] Gorji, S. A., Sahebi, H. G., Ektesabi, M., & Rad, A. B. (2019). Topologies and control schemes of bidirectional DC–DC power converters: An overview. IEEE Access, 7, 117997-118019.

[27] Mumtaz, F., Yahaya, N. Z., Meraj, S. T., Singh, B., Kannan, R., & Ibrahim, O. (2021). Review on non-isolated DC-DC converters and their control techniques for renewable energy applications. Ain Shams Engineering Journal, 12(4), 3747-3763.

[28] Raghavendra, K. V. G., Zeb, K., Muthusamy, A., Krishna, T. N. V., Kumar, S. V. P., Kim, D. H., ... & Kim, H. J. (2019). A comprehensive review of DC–DC converter topologies and modulation strategies with recent advances in solar photovoltaic systems. electronics, 9(1), 31.

[29] Alaql, F., & Batarseh, I. (2019, October). Review and comparison of resonant DC-DC converters for wide-input voltage range applications. In 2019 IEEE Conference on Power Electronics and Renewable Energy (CPERE) (pp. 453-458). IEEE.

[30] Chakraborty, S., Vu, H. N., Hasan, M. M., Tran, D. D., Baghdadi, M. E., & Hegazy, O. (2019). DC-DC converter topologies for electric vehicles, plug-in hybrid electric vehicles and fast charging stations: State of the art and future trends. Energies, 12(8), 1569.

Bibliography

[31] Jotham Jeremy, L., Ooi, C. A., & Teh, J. (2020). Non-isolated conventional DC-DC converter comparison for a photovoltaic system: A review. Journal of Renewable and Sustainable Energy, 12(1).

[32] Baharudin, N. H., Mansur, T. M. N. T., Hamid, F. A., Ali, R., & Misrun, M. I. (2017). Topologies of DC-DC converter in solar PV applications. Indonesian Journal of Electrical Engineering and Computer Science, 8(2), 368-374.

[33] Hossain, M. Z., & Rahim, N. A. (2018). Recent progress and development on power DC-DC converter topology, control, design and applications: A review. Renewable and Sustainable Energy Reviews, 81, 205-230.

[34] Bernardinis, D. (2015). review on DC/DC converter architectures for power fuel cell applications. Energy conversion and management.

[35] Wang, Z., Su, X., Zeng, N., & Jiang, J. (2024). Overview of Isolated Bidirectional DC–DC Converter Topology and Switching Strategies for Electric Vehicle Applications. Energies, 17(10), 2434.

[36] Kabalo, M., Blunier, B., Bouquain, D., & Miraoui, A. (2010, September). State-of-the-art of DC-DC converters for fuel cell vehicles. In 2010 IEEE Vehicle Power and Propulsion Conference (pp. 1-6). IEEE.

[37] Litrán, S. P., Durán, E., Semião, J., & Díaz-Martín, C. (2022). Multiple-output DC–DC Converters: Applications and solutions. Electronics, 11(8), 1258.

[38] Van den Broeck, G., Stuyts, J., & Driesen, J. (2018). A critical review of power quality standards and definitions applied to DC microgrids. Applied energy, 229, 281-288.

[39] Bollen, M. H. (2000). Understanding power quality problems (Vol. 3). New York: IEEE press.

[40] IEEE emerald book, Powering and G rounding E l e c t ronic E q u i p m e n t, Approved 9 December 2005 IEEE-SA Standards Board Approved 29 December 2005 American National Standards Institute.

Bibliography

[41] Marx, D., Magne, P., Nahid-Mobarakeh, B., Pierfederici, S., & Davat, B. (2011). Large signal stability analysis tools in DC power systems with constant power loads and variable power loads—A review. IEEE Transactions on Power Electronics, 27(4), 1773-1787.

[42] R. H. Lasseter, "Microgrids and distributed generation," Intell. Autom. Soft Comput., vol. 16, no. 2, pp. 225–234, 2010.

[43] Singh, S., Gautam, A. R., & Fulwani, D. (2017). Constant power loads and their effects in DC distributed power systems: A review. Renewable and Sustainable Energy Reviews, 72, 407-421.

[44] Ciornei, I., Albu, M., Sanduleac, M., Hadjidemetriou, L., & Kyriakides, E. (2017, June). Analytical derivation of PQ indicators compatible with control strategies for DC microgrids. In 2017 IEEE Manchester PowerTech (pp. 1-6). IEEE.

[45] Asmus, P. (2010). Microgrids, virtual power plants and our distributed energy future. The Electricity Journal, 23(10), 72-82.

[46] Khattab, K., Safa, A., Gouichiche, A., & Messlem, Y. (2022, October). A Comparative Study of Three Methods for Controlling Cascaded Systems in DC Microgrids. In 2022 2nd International Conference on Advanced Electrical Engineering (ICAEE) (pp. 1-5). IEEE.

[47] Derbeli, M., Barambones, O., Ramos-Hernanz, J. A., & Sbita, L. (2019). Real-time implementation of a super twisting algorithm for PEM fuel cell power system. Energies, 12(9), 1594.

[48] Kaplan, O., & Bodur, F. E. R. H. A. T. (2022). Super Twisting Algorithm Based Sliding Mode Controller for Buck Converter Feeding Constant Power Load. International Journal of Renewable Energy Research, 12(1), 134-145.

[49] Riyas, K., & Anasraj, R. (2016, September). Improved performance of boost converter with super-twisting algorithm under sliding-mode operation. In 2016 International Conference on Next Generation Intelligent Systems (ICNGIS) (pp. 1-6). IEEE.

Bibliography

[50] Kim, S., & Williamson, S. S. (2011, September). Negative impedance instability compensation in more electric aircraft DC power systems using state space pole placement control. In 2011 IEEE Vehicle Power and Propulsion Conference (pp. 1-6). IEEE

[51] Chen, Z., & Xu, J. (2014). High boost ratio DC–DC converter with ripple-free input current. Electronics Letters, 50(5), 353-355.

[52] R. Stala, Z. Waradzyn, and S. Folmer, "Input Current Ripple Reduction in a Step-Up DC–DC Switched-Capacitor Switched-Inductor Converter" IEEE Access, vol. 10, 19890–19904, 2022]

[53] Al-Saffar, M. A., & Ismail, E. H. (2015). A high voltage ratio and low stress DC–DC converter with reduced input current ripple for fuel cell source. Renewable Energy, 82, 35-43.

[54] S. Dutta, and B. Johnson, "A Practical Digital Implementation of Completely Decentralized Ripple Minimization in Parallel-Connected DC–DC Converters" IEEE Trans. Power Electron, vol. 37, no. 12, 14422-14433, 2022]

[55] Kim, H. J., Park, Y. M., Son, Y. D., Kang, J. B., Lee, J. Y., & Kim, J. M. (2023). The DC Inductor Current Ripple Reduction Method for a Two-Stage Power Conversion System. Electronics, 12(14), 3005.

[56] R.O. Sanchez, J.Y. Rumbo Morales, G. Ortiz Torres, A.F. Pérez Vidal, J.E. Valdez Resendiz, F.D.J Sorcia Vázquez, and N.V. Nava, "Discrete state-feedback control design with D-stability and genetic algorithm for LED driver using a buck converter", International Transactions on Electrical Energy Systems, 2022]

[57] Xu, Q., Zhang, C., Wen, C., & Wang, P. (2017). A novel composite nonlinear controller for stabilization of constant power load in DC microgrid. IEEE Transactions on Smart Grid, 10(1), 752-761.

[58] Utkin, V. (2013). Sliding mode control of DC/DC converters. Journal of the Franklin Institute, 350(8), 2146-2165.

Bibliography

[59] Hossain, E., Perez, R., Padmanaban, S., Mihet-Popa, L., Blaabjerg, F., & Ramachandaramurthy, V. K. (2017). Sliding mode controller and Lyapunov redesign controller to improve microgrid stability: A comparative analysis with CPL power variation. Energies, 10(12), 1959.

[60] RakhtAla, S. M., Yasoubi, M., & HosseinNia, H. (2017). Design of second order sliding mode and sliding mode algorithms: a practical insight to DC-DC buck converter. IEEE/CAA Journal of Automatica Sinica, 4(3), 483-497.

[61] Benayache, R. (2009). Contribution à la commande robuste des systèmes non linéaires incertains (Doctoral dissertation, Université de Valenciennes et du Hainaut Cambraisis).

[62] Derbeli, M., Barambones, O., Ramos-Hernanz, J. A., & Sbita, L. (2019). Real-time implementation of a super twisting algorithm for PEM fuel cell power system. Energies, 12(9), 1594.

[63] Sira-Ramirez, H. J., & Silva-Ortigoza, R. (2006). Control design techniques in power electronics devices. Springer Science & Business Media.

[64] RobertW, E., & Dragan, M. (2001). Fundamentals of power electronics.

[65] Zhuo, S., Gaillard, A., Li, Q., Ma, R., Paire, D., & Gao, F. (2020). Current ripple optimization of four-phase floating interleaved DC–DC boost converter under switch fault. IEEE Transactions on Industry Applications, 56(4), 4214-4224.

[66] GOUICHICHE, A. (2015). Diagnostic à base d'observateurs et commande tolérante aux défauts (Doctoral dissertation, Alger, Ecole Nationale Polytechnique).

[67] Li, H., Liu, Q., Zhang, Z., Liu, C., Li, Z., Yang, Z., & Zheng, T. Q. (2022). A describing function-based stability analysis method for cascaded DC-DC converters. IEEE Open Journal of the Industrial Electronics Society, 3, 484-495.

[68] Shoja-Majidabad, S. (2020). Flatness-Based Decentralized Adaptive Backstepping Control of Cascaded DC–DC Boost Converters Using Legendre Polynomials. Journal of Control, Automation and Electrical Systems, 31(6), 1533-1548.

Bibliography

[69] Ji, H., Xie, F., Chen, Y., & Zhang, B. (2022). Small-step discretization method for modeling and stability analysis of cascaded DC–DC converters with considering different switching frequencies. IEEE Transactions on Power Electronics, 37(8), 8855-8872.

[70] Z. Chen, W. Yong, and W. Gao, "PI and sliding mode control of a multi -input-multi-output boost-boost converter," WSEAS Trans. Power Syst., vol. 9, pp. 87–102, 2014

[71] Li, F., & Lin, Z. (2021). Novel passive controller design for enhancing boost converter stability in DC microgrid applications. IEEE Journal of Emerging and Selected Topics in Power Electronics, 9(6), 6901-6911.

[72] Samadian, A., Hashemzadeh, S. M., Marangalu, M. G., Maalandish, M., & Hosseini, S. H. (2021). A new dual-input high step-up DC–DC converter with reduced switches stress and low input current ripple. IET Power Electronics, 14(9), 1669-1683.

[73] Khan, S., Zaid, M., Mahmood, A., Nooruddin, A. S., Ahmad, J., Alghaythi, M. L., ... & Lin, C. H. (2021). A new transformerless ultra high gain DC–DC converter for DC microgrid application. IEEE Access, 9, 124560-124582.

[74] Nupur, N., & Nath, S. (2019). Minimizing ripples of inductor currents in coupled SIDO boost converter by shift of gate pulses. IEEE Transactions on Power Electronics, 35(2), 1217-1226.

[75] Al-Saffar, M. A., & Ismail, E. H. (2015). A high voltage ratio and low stress DC–DC converter with reduced input current ripple for fuel cell source. Renewable Energy, 82, 35-43

[76] Khattab, K., Safa, A., Gouichiche, A., & Messlem, Y. et al. An Improved Current Ripples Minimization Technique for Cascaded DC–DC Converter in DC Microgrid. Electrica, 2024, vol. 24, no 2.

.

Abstract

ملخص الأطروحة

تركز هذه الأطروحة على تحسين جودة الطاقة في محولات التيار المستمر، استنادًا إلى شبكة تيار مستمر صغيرة تتكون من تركز هذه الأطروحة على تحسين جودة الطاقة في محولات التيار المستمر، استنادًا إلى شبكة تيار مستمر صغيرة تتكون من سلسلة تعاقبية من محولين للتيار المستمر. الهدف هو تحسين جودة الطاقة مع تقليل التذبذبات غير المرغوب فيها في أنظمة التيار المستمر.

تم تطوير نموذج نظري لتقنية تقليل التموج في الشبكة المصغرة للتيار المستمر. ولتقييم فعاليتها، تم إجراء العديد من الاختبارات، وتحليل تأثير المكاسب ومستويات الطاقة والأحمال المتغيرة. تحققت هذه الاختبارات من قدرة النظام على الحفاظ على جودة الطاقة في ظل ظروف مختلفة.

بعد ذلك، تم إعداد نموذج تجريبي للتحقق من صحة التقنية المقترحة. وتعد هذه العملية الجديدة، التي تعتمد على الاختيار الصحيح للسطح المنزلق، نهجًا مبتكرًا للتخميد النشط، ولا تتطلب أجهزة استشعار إضافية ولا مكونات سلبية، مما يساعد على تقليل التكاليف. وقد أكدت النتائج التجريبية التحسن في جودة التيار والجهد، بالإضافة إلى متانة النظام أمام تغيرات الجهد. هذه الطريقة سهلة التنفيذ ويمكن تطبيقها على أنواع مختلفة من الأحمال ومستويات الطاقة.

Abstract

This thesis focuses on the improvement of power quality in DC-DC converters, based on a DC microgrid consisting of a cascade of two DC-DC converters. The aim is to improve power quality while reducing undesirable oscillations in DC systems.

A theoretical model of a ripple minimization technique in the DC microgrid has been developed. To evaluate its effectiveness, several tests were carried out, analyzing the effect of varying gains, power levels and loads. These tests verified the system's ability to maintain power quality under various conditions.

Next, an experimental prototype was set up to validate the proposed technique. This new process, based on the correct choice of sliding surface, is an innovative approach to active damping, requiring neither additional sensors nor passive components, which helps to reduce costs. Experimental results have confirmed the improvement in current and voltage quality, as well as the robustness of the system to voltage variations. The method is easy to implement and can be applied to different types of loads and power levels.

Résumé

Cette thèse est axée sur l'amélioration de la qualité de l'énergie dans les convertisseurs DC-DC, sur la base d'un micro-réseau DC constitué d'une cascade de deux convertisseurs DC-DC. L'objectif est d'améliorer la qualité de l'énergie tout en réduisant les oscillations indésirables dans les systèmes CC.

Un modèle théorique d'une technique de minimisation de l'ondulation dans le micro-réseau CC a été développé. Pour évaluer son efficacité, plusieurs tests ont été effectués, analysant l'effet de la variation des gains, des niveaux de puissance et des charges. Ces tests ont permis de vérifier la capacité du système à maintenir la qualité de l'énergie dans diverses conditions.

Ensuite, un prototype expérimental a été mis en place pour valider la technique proposée. Ce nouveau procédé, basé sur le choix correct de la surface de glissement, constitue une approche innovante de l'amortissement actif, ne nécessitant ni capteurs supplémentaires ni composants passifs, ce qui contribue à réduire les coûts. Les résultats expérimentaux ont confirmé l'amélioration de la qualité du courant et de la tension, ainsi que la robustesse du système aux variations de tension. La méthode est facile à mettre en œuvre et peut être appliquée à différents types de charges et de niveaux de puissance.